Distribution Category:
Energy Conversion
(UC-93)

ANL-83-89

ARGONNE NATIONAL LABORATORY
9700 South Cass Avenue
Argonne, Illinois 60439

ANL--83-89

DE84 008964

ADVANCED FUEL CELL DEVELOPMENT

Progress Report for
April—June 1983

J. P. Ackerman, Manager, Electrochemical Research
R. D. Pierce, Molten Carbonate Fuel Cell Group Leader
D. C. Fee, Solid Oxide Fuel Cell Group Leader

Chemical Technology Division

DISCLAIMER

February 1984

LIST OF CONTRIBUTORS

The following is a list of contributors to this report. Included are Argonne National Laboratory personnel as well as contributors with other affiliations, as indicated.

T. D. Claar (ANL, Materials Science and Technology Division)
J. T. Dusek (ANL, Materials Science and Technology Division)
T. Fannon (Student researcher, Tennessee Technological University, Cookeville, TN)
R. J. Fousek (ANL, Materials Science and Technology Division)
T. D. Kaun
N. Q. Minh
F. C. Mrazek
P. E. Papierski (Resident student associate, University of Illinois Medical School, Chicago, IL)
S. Peterson (Undergraduate research participant, Rensselaer Polytechnic Institute, Troy, NY)
J. J. Picciolo (ANL, Materials Science and Technology Division)
D. Pickrell (Undergraduate research participant, Ohio State University, Columbus, OH)
R. B. Poeppel (ANL, Materials Science and Technology Division)
V. L. Richards (Asst. Professor, Illinois Institute of Technology, Chicago, IL)
J. H. Schoenung (Summer student, University of Illinois, Champaign, IL)
J. W. Sim
J. P. Singh (ANL, Materials Science and Technology Division)
J. L. Smith
J. R. Stapay
R. K. Steunenberg
E. H. Van Deventer
S. A. Zwick

TABLE OF CONTENTS

LIST OF FIGURES

LIST OF FIGURES (contd)

LIST OF TABLES

ADVANCED FUEL CELL DEVELOPMENT

Progress Report for
April-June 1983

ABSTRACT

This report describes research and development activities on both molten carbonate and solid oxide fuel cells at Argonne National Laboratory (ANL) during the period April through June 1983. The efforts on development of molten carbonate fuel cells have been directed principally toward seeking alternative cathode materials to NiO. Based on an investigation of the thermodynamically stable phases formed under cathode conditions with a number of transition metal oxides, synthesis of prospective alternative cathode materials and doping of these materials to promote electronic conductivity is under way. The compounds $LiFeO_2$, Li_2MnO_3, and ZnO have been doped to give suitable conductivity. These are further tested for solubility and ion migration in the cell environment. In addition, solubility data were taken for NiO, CoO, and NiO-CoO in a cathode environment with different carbonate-salt compositions. Techniques are being studied for the preparation of thin electrode and electrolyte materials by tape-casting, and a creep-resistant superstructure for the anode is under development. The objective of the work on solid oxide fuel cells is development of an advanced, high-power-density fuel cell. By employing the thin ceramic layer components of existing solid oxide fuel cells in a strong, lightweight structure of small cells, unequaled power per unit mass or volume can be achieved. During this report period, work was done on advanced electrolyte fabrication, electrolyte sintering studies, and interconnection and electrode fabrication.

SUMMARY

Molten Carbonate Fuel Cells

Because of the problem of NiO cathode dissolution in molten carbonate fuel cells (MCFCs), the MCFC experimental work at Argonne has concentrated principally on the investigation of alternative cathode materials. In addition, some preliminary work has been devoted to the solution of an anode creep problem that has also been troublesome.

Cathode Development--Alternative Cathode Materials

The major problem in selecting an alternative cathode material is achieving the required stability in the fuel cell environment. Accordingly, the major emphasis is on investigating compounds that are found to be thermodynamically stable under cathode conditions. Research is under way to promote conductivity in these oxides by doping. Resistivities are determined on porous sintered samples using the van der Pauw procedure, and stability is further assessed in solubility and migration tests.

Magnesium- and zinc-doped $LiFeO_2$ were prepared. To date, the samples have shown high resistivity (about 500 Ω•cm at 925 K). Some samples were contaminated with about 0.5 wt % aluminum during a grinding step, but this had no detectable effect on the conductivity. Work is under way to optimize manganese-doped $LiFeO_2$; samples prepared earlier had promising resistivities (5 Ω•cm at 925 K).

The effects of dopant concentration and the method of preparation for magnesium-doped Li_2MnO_3 are under investigation. Improvements have been introduced to eliminate problems of incomplete precipitation and loss of material during washing steps.

Resistivity measurements were made on ZnO doped with chromium or zirconium. The resistivity of a sample doped with 2 mol % chromium was about 2 Ω•cm, and that for a 3 mol % zirconium-doped sample was about 3.5 Ω•cm at 925 K. These resistivities are probably adequate for application as cathodes. A similar resistivity was reported last quarter for aluminum-doped ZnO. We are concerned about the possible poisoning of the conductivity by in situ doping by lithium in the fuel cell. Accordingly, experiments have been performed to investigate in situ doping. No significant lithium has been introduced in the ZnO, and no effect was observed on the conductivity of an aluminum-doped sample.

Synthesis of Li_2SnO_3 has been initiated, and samples of magnesium- and iron-doped material have been prepared. Considerable difficulty was encountered with filtering and washing samples and with equipment corrosion, but acceptable procedures have been developed, and samples have been prepared for conductivity testing.

Evaluation of Cathode Materials

Apparatus has been built to test the migration of materials in a simple fuel cell. An evaluation of the electrolyte structure for materials accumulation is the principal analytical approach. The first tests were run with tape-cast cathodes of NiO and Li_2MnO_3. The expected nickel precipitates were observed with the NiO cathode, but no manganese-containing precipitates were found with the Li_2MnO_3 cathode. The apparatus is being modified to improve its performance, and testing of candidate cathodes will continue.

Preliminary results of NiO solubility in dry 75 mol % Li_2CO_3-K_2CO_3 indicate <10 wppm for the temperature range 873 to 1023 K. This is substantially lower than the solubility in the standard 62 mol % Li_2CO_3-K_2CO_3. The effect of humidity on the solubility is also less for the higher lithium composition. The solubility ranged from 20 to 50 wppm for temperatures from 873 to 1073 with 3% moisture.

A new pot-type solubility apparatus is in operation. Samples are contained in an Al_2O_3 crucible with 45 cm^3 of carbonate melt. Each crucible contains a purge gas bubbler that provides gentle circulation of the melt as well as promoting equilibrium between the cover gas and the melt. Initial tests examined NiO, CoO, and $NiCoO_2$ in two Li/K ratios, under dry and humid conditions with 30% CO_2-air purge.

Anode Development

Development of a creep-resistant anode structure is sought through application of low-surface-area foam metal as a superstructure for the anode. This strong, highly porous matrix provides a gas-flow passage with little masking of electrode and electrolyte area. Integrated structures have been fabricated with the bipolar sheet brazed onto the foam metal which has the anode embedded in it.

Ceramic Materials Development

Techniques are being developed for the fabrication of porous pellets for stability testing of cathode materials. Pellets of $LiFeO_2$ and Li_2MnO_3 were prepared and sintered at 1175 and 1475 K. The Li_2MnO_3 pellets exhibited no significant densification (about 40% porosity) at either temperature, but a much stronger product was formed at the higher temperature. The $LiFeO_2$ densified from 42 to 29% porosity at the higher temperature. Additional pellets of about 40% porosity will be produced for stability testing, and the effort will be expanded to include ZnO.

The fabrication of thin electrolyte support matrices by both conventional tape-casting and powder-rolling processes is being evaluated. Both $LiAlO_2$ synthesized in-house and commercial material are being used. Samples of commercial $LiAlO_2$ have been sent to several outside vendors to evaluate the capability of their equipment to jet mill the agglomerates to the desired submicron particle size range.

MCFC Systems Code

A systems code, SALT, is used at ANL to analyze MCFC power plants. Recently, considerable analysis has been performed for methane-fueled plants, and for some runs, convergence of the chemical equilibria calculations involving methane reforming was very slow. The problem seems to have been solved by modifications to refine initial estimates prior to the detailed equilibrium calculations.

Advanced Concept Development for Solid Oxide Fuel Cells

Background

The objective of the work on solid oxide fuel cells is to develop an advanced, high-power-density fuel cell. The unique fuel cell design achieves unequaled power per unit mass or volume by employing the thin ceramic layer components of existing solid oxide fuel cells in a strong, lightweight structure of small cells. It will convert hydrocarbon fuels to dc power at ≥45% efficiency, and so can achieve considerably higher energy densities than other technologies that use nonexotic fuels.

Advanced Fabrication

Electrolyte Fabrication

The electrolyte fabrication effort was focused on the development of tape-casting procedures for the preparation of Y_2O_3-stabilized ZrO_2 electrolyte. These investigations involved the use of Zircar Type ZYP

zirconia, which is stabilized with 16 wt % yttria, and the Cladan No. 73200 binder system, which uses isopropanol as the solvent with a vinyl binder. Severe agglomeration of the finely divided (<0.1 μm) zirconia, which occurred when isopropanol alone was used as the solvent in the preparation of slips, was nearly eliminated when a 40 wt % water-60 wt % isopropanol solution was used as the solvent.

A procedure is being developed for the removal of chloride impurities from the Zircar zirconia. Chloride, which is present at a concentration of about 0.8 wt %, raises the sintering temperature of the material by approximately 150°C and may be related to the formation of agglomerates.

Electrolyte Sintering Studies

The near-term objective of this work is to define the experimental conditions required to provide a thin sheet (~0.001-in. (0.025-mm) thick) of high-density (>95%) Y_2O_3-stabilized ZrO_2. The longer-term objective is to produce a composite structure containing one or more porous electrode layers and a dense Y_2O_3-stabilized ZrO_2 electrolyte layer. The effort focuses on tape casting and sintering. Each step in the fabrication process is briefly discussed.

Interconnection and Electrode Fabrication

The interconnection and electrode fabrication effort focused on developing tape-casting methodology for thin electrode and interconnection layers and developing slip-casting and extrusion technology for electrode layers. Thin [1-2 mil (0.025-0.051 mm)] layers of interconnection material [$La(Cr_{0.9}Mg_{0.1})O_3$] with the desired porosity (less than 10%) have been fired at 1550°C in a reducing atmosphere. Thin layers of anode [50 vol % Co/50 vol % ZrO_2] and cathode [$(La_{0.9}Sr_{0.1})MnO_3$] materials with the desired porosity (30-50%) have been fired at 1200 to 1300°C in air. Measurements show a good thermal expansion match for these materials. The mean thermal expansion coefficients (25 to 1000°C) were determined as 10.6×10^{-6}/°C for the air electrode, 9.6×10^{-6}/°C for the interconnection, and 10.3×10^{-6}/°C for the ZrO_2-16 wt % Y_2O_3 electrolyte. Anode and cathode pieces containing gas flow channels have been fabricated by slip-casting and extrusion techniques. The extrusion methodology appears to be readily adaptable to the formation of anode and cathode in the high-power-density, monolithic fuel cell.

Electrical Conductivity Measurements in Ceramics

The conductivity of the ceramic layers is an important property of the monolithic fuel cell. The conductivity and efficiency are diminished if highly resistive phases or contact resistances develop at the interface between ceramic layers. Measurements of the electronic and ionic conductivity of components of the monolithic cell can be accomplished by a variety of techniques. Frequency-dependent impedance methods appear to offer the most promise for characterizing the conductivity across a ceramic interface.

I. INTRODUCTION

The advanced fuel cell studies at Argonne National Laboratory (ANL) are part of the DOE Advanced Fuel Cell Program. The objective of this DOE program is to reduce the technical uncertainties of fuel cells so that manufacturers and users can introduce high-efficiency generating systems which have the capability of operating on coal or other fuels. At the present stage of development, the primary thrust of the ANL program is to provide supporting research and development that pursues fundamental understanding of fuel cell behavior and investigates alternative stack concepts.

At ANL, work is concentrated on the development of the molten carbonate fuel cell (MCFC) and on advanced design concepts for solid oxide fuel cells (SOFCs).

The underlying reasons for developing MCFC and SOFC power plants are the following: (1) they are capable of meeting baseload as well as intermediate (cycling) electrical energy requirements and of cogenerative power with industrial coal-consuming generators; (2) the cost of the electricity they generate is projected to be fully competitive with other types of power plants; and (3) their projected efficiency is 45% or higher on coal fuel. This efficiency is higher than competitive power plants and should result in decreased coal demand per unit electric energy.

II. DEVELOPMENT OF MOLTEN CARBONATE FUEL CELLS

A. Introduction

The present molten carbonate fuel cells consist of a porous nickel anode, a porous lithiated nickel oxide cathode, an electrolyte structure which separates the anode and cathode and conducts only ionic current between them, and appropriate metal housings or, in the case of stacks of cells, intercell separator sheets. The cell housings (or separator sheets) bear upon the electrolyte structure to form a seal between the environment and the anode and cathode gas compartments. The usual electrolyte structure is a composite of discrete $LiAlO_2$ particles and a mixture of alkali metal carbonates. The carbonates are liquid at the cell operating temperature of about 925 K. At the anode, hydrogen and carbon monoxide in the fuel gas react with carbonate ion from the electrolyte to form water and carbon dioxide while giving up electrons to the external circuit. At the cathode, carbon dioxide and oxygen react and accept electrons from the external circuit to form carbonate ion, which is conducted through the electrolyte to the anode. In a practical cell stack, CO_2 for the cathode probably would be obtained from the anode exhaust.

It has become apparent that for pressurized operation, which is desirable for large power plants, nickel dissolution from the NiO cathode and deposition of metallic nickel in the electrolyte will preclude the 4×10^4-h lifetime desired for commercial cells. The evaluation of possible alternative cathode materials is the group's principal activity at present. We are also considering ways to obtain satisfactory cell life with NiO cathodes.

Cells are operated to assess the behavior of components and to understand the performance of life-limiting mechanisms at work within the cell. Cell operation is coupled with efforts in diagnostics and materials development.

B. Cathode Development--Alternative Cathode Materials

(J. L. Smith, N. Q. Minh, E. H. Van Deventer, and J. H. Schoenung*)

The major problem in selecting a cathode material is achieving the required material stability in the fuel cell environment. Accordingly, our major emphasis is on investigating compounds that are found to be thermodynamically stable in a cathode environment. Research is under way to improve conductivity in these compounds by incorporating appropriate dopants and to determine if the resulting materials have adequate stability. The stability is evaluated in solubility and migration tests and by examination of samples for microstructural or compositional changes.

1. $LiFeO_2$

Resistivity measurements† were made on one Zn- and four Mg-doped samples of $LiFeO_2$. All were prepared by coprecipitation; details of the preparations are discussed below.

---

*Summer student from the University of Illinois, Champaign, IL.

†All resistivity measurements were made using the van der Pauw technique!

Two samples, one of Mg- and one of Zn-doped $LiFeO_2$, were prepared by adding sufficient NH_4OH to an aqueous solution of the appropriate nitrates to bring the pH to ∿10. After centrifugation, the precipitates were washed well with H_2O and dried at ∿150°C in air. They were then heated to 1000°C in air for ∿12 h. The samples were then reacted with Li_2CO_3/K_2CO_3 eutectic at 700°C in an atmosphere of 30% CO_2, balance air. The products of this step were then ground and washed with water until a neutral pH was achieved. Inductively coupled plasma (ICP) analysis showed nominal compositions of $Li_{0.94}Mg_{0.07}FeO_2$, and $Li_{0.92}Zn_{0.13}FeO_2$. These formulas are based solely on an analysis for the cations and assume single phases. Both samples contained significant Al--0.78 and 0.44 wt %, respectively. This aluminum content was traced to the grinding step. Samples of these materials were cold-pressed with paraffin binder and sintered at 1300°C for 1 h. The resistivity of these pellets is shown in Fig. 1.

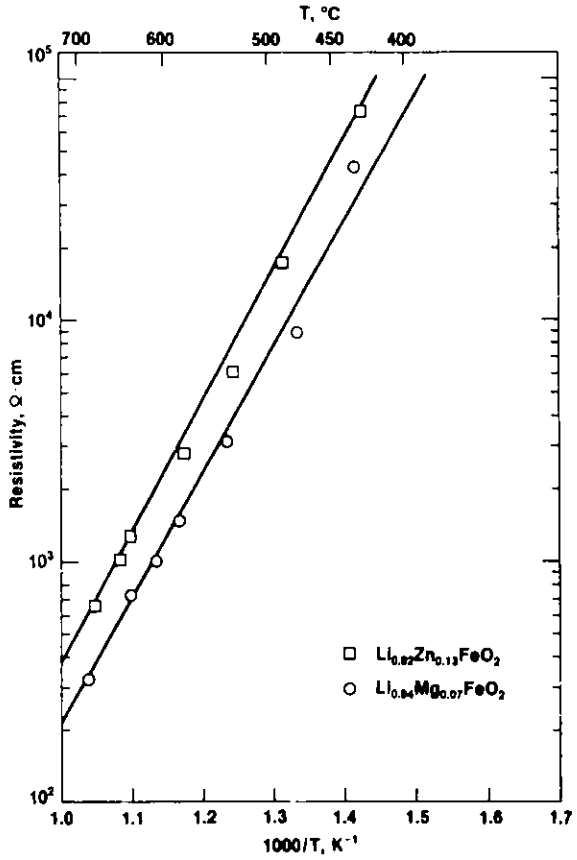

Fig. 1.

Resistivity of Doped $LiFeO_2$

Each of the next three coprecipitates was prepared slightly differently. Sample A-15-1 was prepared by adding NH_4OH dropwise to an aqueous solution of iron and magnesium nitrates; sample A-17-1 was prepared by adding the nitrate mixture to the NH_4OH; and sample A-19-1 was prepared by adding the nitrate mixture to KOH. For the latter sample, KOH was used as a precipitant to see if we could more closely approach the desired composition. Ammonium hydroxide produces a buffered solution which may affect the precipitation. Moreover, since the precipitates are subsequently reacted with K_2CO_3 and Li_2CO_3, the use of either KOH or LiOH in place of NH_4OH should be inconsequential.

Following coprecipitation, samples A-15-1, A-17-1, and A-19-1 were filtered in a Buchner funnel. The filter cakes were removed, blended with distilled H_2O, and refiltered. This process was repeated until the pH of the wash water was neutral. The final material was then dried at ~150°C in air, pulverized, and carbonate-treated for 100 h at 700°C as previously described. (The interdiffusion step was bypassed.) After the respective residues were washed with water to remove the carbonate, the samples were dried, made into pellets, and sintered at 1100°C for 1 h. The measured electrical resistivity of these pellets is shown in Fig. 2. After these results were obtained, the pellets were resintered at 1300°C for 1 h and the resistivity was measured. There was no significant change in resistivity. The nominal compositions indicated by chemical analyses (ICP) for the cations of the samples are as follows: A-15-1, $Li_{0.98}Mg_{0.049}Fe_{0.99}O_2$; A-17-1, $Li_{0.95}Mg_{0.084}Fe_{0.98}O_2$; and A-19-1, $Li_{0.89}Mg_{0.20}Fe_{0.90}O_2$. These formulas are based on the existence of only one phase. (No significant Al_2O_3 was present since the grinding step was bypassed.)

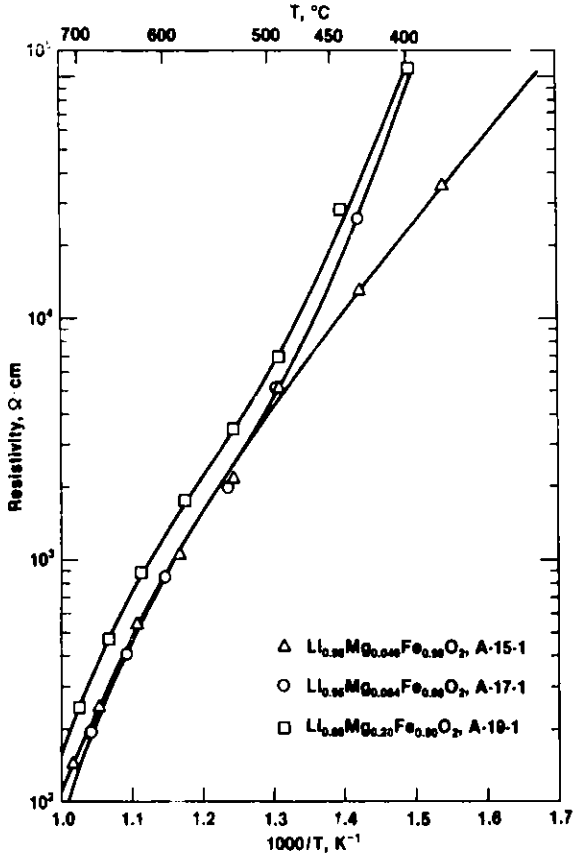

Fig. 2.

Resistivity of Magnesium-Doped $LiFeO_2$

To date, good conductivity has not been achieved with Mg-doped $LiFeO_2$, possibly due to the substitution of magnesium for both Li and Fe. Nevertheless, several things have been learned: (1) although Al_2O_3 was previously introduced in grinding, it appears to be benign and does not interfere with resistivity measurements or alter conductivity, (2) coprecipitation with either LiOH or KOH appears to be a viable alternative to NH_4OH, and (3) X-ray diffraction (XRD) of the coprecipitate shows no pattern and thus indicates that a very fine particle size exists.

Preliminary resistivity measurements on Mn-doped $LiFeO_2$ gave promising results. Preparation of and resistivity measurements on a series of Mn-doped ferrites are in progress. In addition, some of the Mn- and Mg-doped material that has not been carbonate-treated will be calcined and then carbonate-treated to determine if such treatment is beneficial.

2. Li_2MnO_3

Attention has centered on examining the effect of varying amounts of magnesium dopant in Li_2MnO_3. It was found that the procedures being used for the precipitation of magnesium and manganese hydroxides from a nitrate solution did not result in a predictable amount of dopant in the samples.

The procedure consisted of adding manganese/magnesium nitrate solution dropwise to a LiOH or NH_4OH solution stirred in a blender. Both ammonium hydroxide and lithium hydroxide solutions were used in approximately stoichiometric quantities. After precipitation, the samples were filtered, and the filter cake washed to remove the nitrates.

The cause of the problem with dopant concentration appears to be that in some cases the magnesium was not completely precipitating, and in others it was redissolving during the washing step. The best procedure seems to be to do both the precipitation and wash using an excess of base. In the case of ammonium hydroxide, a buffered solution is formed, but the goal stoichiometry is attained. With lithium hydroxide, both the precipitation and wash were done at a pH of ~10.

Two samples are currently being reacted with carbonates. These have an Mn/Mg ratio of 10:1 and 20:1. Several earlier samples with a 5:1 ratio had resistivities of <10 Ω•cm at 650°C in air. Samples of materials with Mn/Mg ratios of up to 90:1 have been prepared but not yet tested for resistivity.

3. ZnO

Our short-term (100-h) stability tests indicated the stability of ZnO to the Li_2CO_3-K_2CO_3 melt under the cathode conditions. In order to evaluate ZnO as a suitable material for use as a MCFC cathode, work has been carried out on synthesizing ZnO doped with various dopants (Al, Cr, and, Zr) and determining the electronic resistivity of the doped compounds. During this reporting period, samples of ZnO doped with chromium and zirconium were prepared and tested for resistivity.

a. Cr-Doped ZnO

Chromium-doped ZnO was prepared by two methods: from ZnO powder + $Cr(NO_3)_3$ solution and from hydroxide coprecipitates of $Cr(NO_3)_3$ and $Zn(NO_3)_2$ solution. Heat treatment of Cr-doped ZnO was carried out at 1150°C for 100 h. Figure 3 gives the electronic resistivity at different temperatures of four Cr-doped ZnO discs (first method) sintered at 1150°C for 3 h (about 45% porous); the ZnO had been doped with 2, 3, 4, and 6 mol % Cr_2O_3. Unexpectedly for these samples, low levels of chromium doping resulted in a sharp increase of the electrical resistivity compared to undoped ZnO in air.

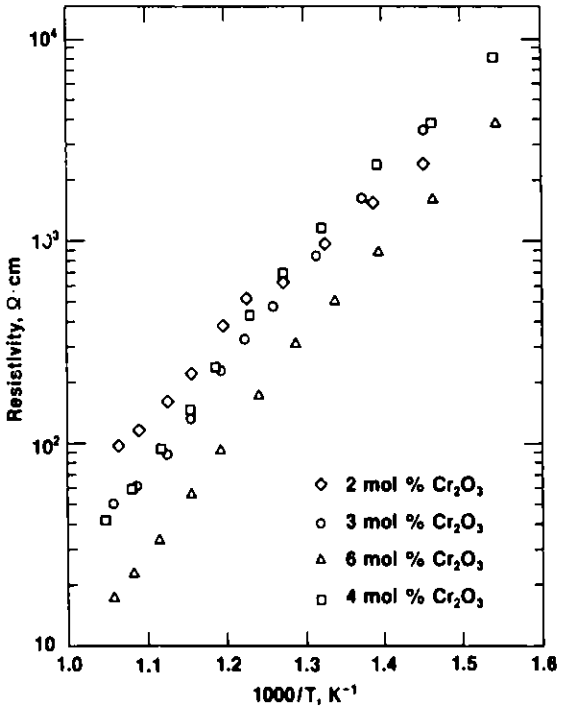

Fig. 3.

Plots of Resistivity of Chromium-Doped ZnO as a Function of Inverse Temperature. (Samples were lightly sintered at 1150°C.)

The resistivity of the doped samples decreases with increasing chromium content. A similar trend is also observed for Cr-doped ZnO samples prepared by coprecipitation and sintered at 1150°C for 3 h (Fig. 4). Experiments to assess the effect of sintering on the conductivity of Cr-doped ZnO were carried out. Pellets from the materials from ZnO powder + $Cr(NO_3)_3$ solution

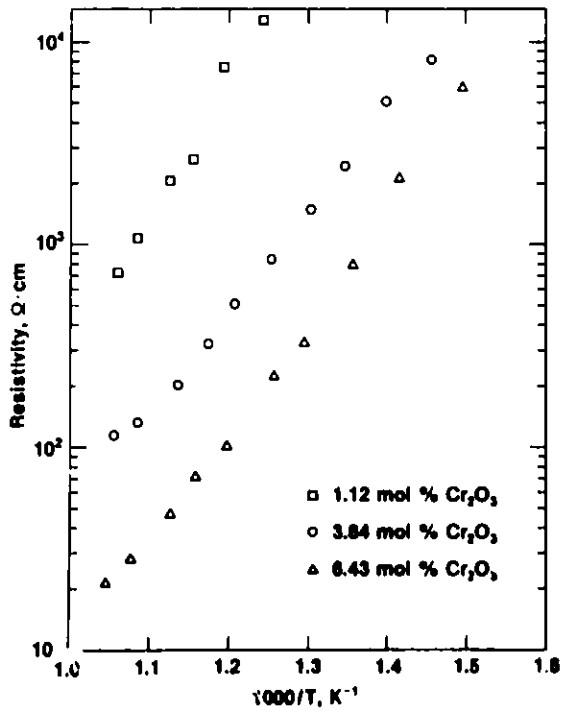

Fig. 4.

Resistivity of Chromium-Doped ZnO (prepared by coprecipitation) at Different Temperatures. (Samples were lightly sintered at 1150°C.)

were prepared and sintered at 1300°C for 3 h. The porosity of these pellets after sintering was about 45%. The results of resistivity measurements are shown in Fig. 5. It can be seen that pellets sintered at 1300°C (Fig. 5) show much lower resistivities than those that were only lightly sintered at 1150°C (Fig. 3). Also, the resistivity increases with increasing chromium content from 2 to 4 mol %, reversing the trend observed for samples sintered at 1150°C. The observed behavior of the resistivity as a function of chromium content of the samples sintered at 1150°C may be an anomaly due to sintering effects. Experiments on the effect of sintering temperature on the resistivity of chromium-doped ZnO prepared by coprecipitation are in progress.

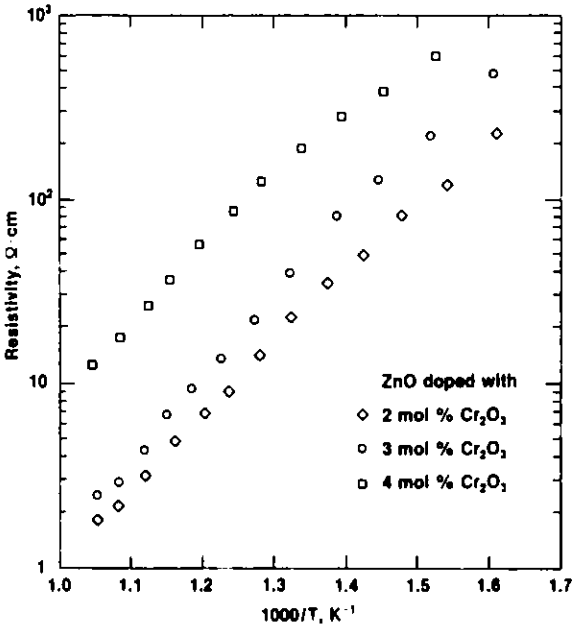

Fig. 5.

Resistivity of Chromium-Doped ZnO Sintered at 1300°C.

b. ZrO-Doped ZnO

The preparation of Zr-doped ZnO was as follows. Zinc oxide powder was added to aqueous $Zr(NO_3)_4$. The slurry was stirred, filtered, dried in air, ground, calcined in air at 1000°C for 3 h, and ground again. The resulting powder was pressed into pellets and sintered at 1300°C for 3 h. The sintered pellets were pale yellow. Analysis by X-ray diffraction* of the doped ZnO sample showed that, in addition to the ZnO phase, $ZrZnO_3$ was present as a minor phase. In Fig. 6, the resistivity measured in air is shown as a function of inverse temperature for ZnO doped with 1, 2, 3, 4, and 6 mol % ZrO_2. As seen from the figure, the resistivity-temperature characteristics of sintered ZnO bodies doped with zirconium appeared to show a maximum at about 527°C (1.25×10^{-3} K^{-1}). A similar behavior was also

*X-ray diffraction done by B. Tani, Analytical Chemistry Laboratory, ANL.

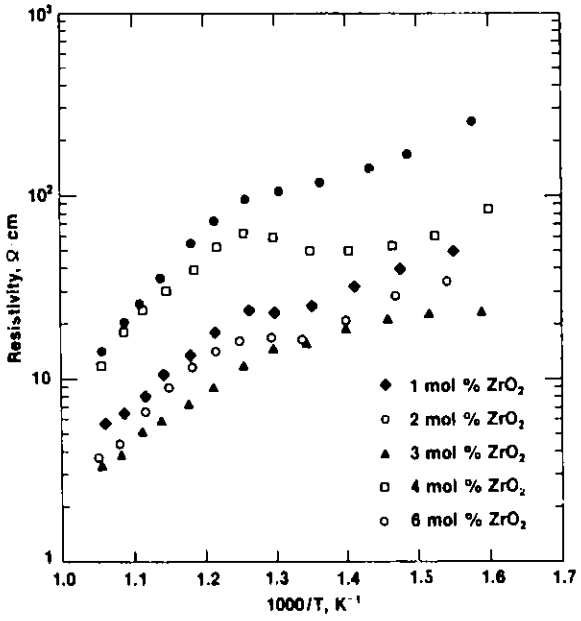

Fig. 6.

Resistivity of Zirconium-Doped ZnO at Different Temperatures

observed for Al-doped ZnO. Compared with undoped ZnO, Zr-doped ZnO is lower in resistivity. Zinc oxide doped with 3 mol % ZrO_2 shows resistivities that may be low enough for use as a cathode material. For example, the resistivity of 3 mol % Zr-doped ZnO was about 4 Ω•cm at 650°C. From the experimental data obtained, it also appears that the optimum Zr dopant concentration (i.e., minimum sample resistivity) is about 3-4 mol %. Synthesis of Zr-doped ZnO by the coprecipitation method was also carried out. Coprecipitates of Zn/Zr hydroxides (or hydrated oxides) were prepared by dropwise addition of an ammonia solution to the stirred Zn/Zr nitrate solution. The coprecipitates were then washed and calcined in air at about 900°C for 3 h to convert the hydroxides to the oxides. Pellets of the resulting powder were pressed and sintered at 1300°C for 3 h. The results of resistivity measurements on these samples are shown in Fig. 7. As seen from Figs. 6 and 7, the coprecipitation preparation yielded a product with poorer conductivity than the (ZnO powder + Zr nitrate) preparation. Not enough information is available at this point to explain this. However, it appears that coprecipitation samples did not sinter as well. Their porosity was about 44% compared with about 20% for samples from the (ZnO powder + zirconium nitrate) preparation. This partly explains the differences in resistivity. Scanning electron microscopy (SEM) analysis is being run on fracture surfaces of the specimens to see if there is any difference in grain size of sintered materials prepared by the two methods. The effect of sintering temperature on the conductivity of precipitated material is also being investigated.

c. The Effect of Lithium Incorporation

Because ZnO is an n-type semiconductor, lithium incorporation is detrimental to its electrical conductivity. The lithium doping of ZnO may occur from contact with the carbonate electrolyte under cathode conditions. The effect on the electrical conductivity of introducing lithium under cathode conditions into doped ZnO is being investigated.

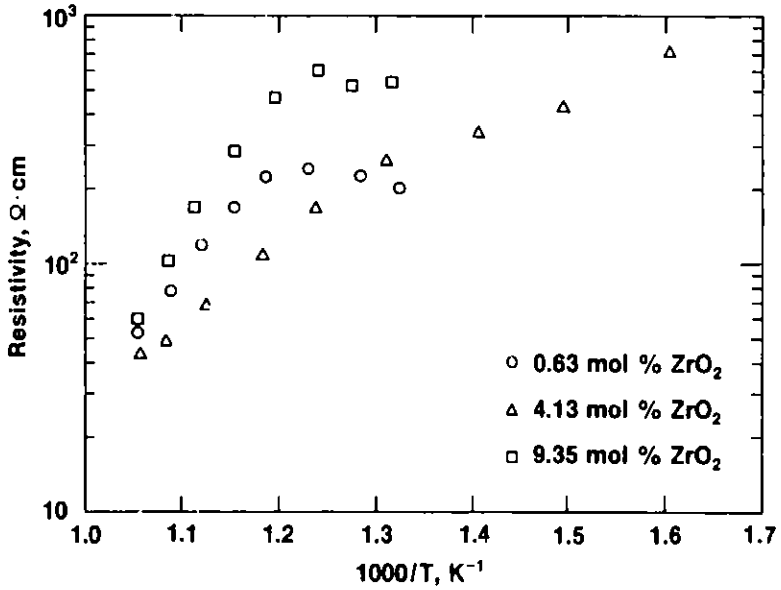

Fig. 7. Resistivity of Zirconium-Doped ZnO Prepared by Coprecipitation

Samples of ZnO doped with Al_2O_3 were treated with excess carbonates at 700°C in a cathode gas environment for 50 h. After the carbonates had been washed off with water, the samples were analyzed for lithium content. It is found that the lithium content of these samples is very low (<10 ppm). As expected, this low lithium content has a negligible effect on the conductivity of doped ZnO. Sintered pellets with and without added lithium (LiOH solution was used to add the desired amount of lithium to the samples) show about the same conductivity. More experiments (at longer times and experiments with chromium- and zirconium-doped ZnO) are being carried out to confirm this result.

4. Li_2SnO_3

Synthesis of Li_2SnO_3 samples has been initiated. Two dopants, Mg^{2+} and Fe^{3+}, have been incorporated into the system. Three different mixing procedures have been used. Due to the difficulties encountered in synthesis, no resistivity measurements have yet been taken.

The first preparation attempted was of the Mg-doped material, $Li_{1.8}Mg_{0.2}SnO_3$. An appropriate amount of solid SnO_2 particles (-100 mesh) was mixed with LiOH in H_2O. A dilute solution of $Mg(NO_3)_2$ was added dropwise to the $LiOH/SnO_2$ mixture with stirring in a blender. The resulting precipitate was filtered and washed with dilute aqueous LiOH.

After the precipitate was dried, half of the batch was heat-treated at 1100°C for 100 h. Both samples were then mixed with excess Li_2CO_3 and heated to 700°C for 100 h in cathode gas. After the solids were ground, they were washed repeatedly with H_2O until the wash had a neutral pH. This took longer than expected, both in filtering time and in number of washings, especially for the sample that had not been heat-treated to 1100°C.

The sample that had not been heat-treated was examined with X-ray analysis.* Three phases were found: Li_2SnO_3, SnO_2, and MgO. The X-ray analysis has not yet been completed on the heat-treated sample. This sample should have better homogeneity and less MgO as a separate phase. Pellets have been made from each sample. Resistivity measurements will be taken after sintering.

A second preparation of doped material was done in a different way. In this case, $Li_{1.8}Fe_{0.2}SnO_3$ was the desired product. The required amounts of $FeCl_3 \cdot 5H_2O$ and $SnCl_4 \cdot 6H_2O$ were dissolved in H_2O. Ammonium hydroxide (55 vol % NH_4OH/45 vol % H_2O) was added dropwise to the aqueous chloride solution in a blender with continuous mixing. Enough NH_4OH was added to bring the solution to a pH of about 3. At this point, a milky green, well-suspended precipitate had formed. It was filtered with much difficulty and then washed alternately with NH_4NO_3 and H_2O until the filtrate was free of chloride. After the solids were dried in air at ~150°C, a sample was analyzed, and a significant amount of Cr was found. It was concluded that the blender blades had been attacked by the acidic solution. Another sample, which had not been washed to remove chloride, was heated to 400°C and analyzed. All of the chloride had been burned off as NH_4Cl, which sublimes at 335°C. This method appears to be an easier way to remove the chloride than by the NH_4NO_3 washings.

Another attempt was made to prepare $Li_{1.8}Fe_{0.2}SnO_3$. The following changes were made in the previous procedure. (1) A glass beaker and stirrer were used to eliminate the chromium impurity. (2) The entire system was heated in a steam bath throughout the precipitation process. (3) The neutralization of chloride was accomplished by adding NH_4OH instead of by monitoring pH. (4) The precipitate was isolated by centrifugation and then heated at 600°C until the NH_4Cl was burned off and SnO_2 was formed. [Stannic oxide (SnO_2) hydrolyzes when formed; i.e., it forms a gelatinous precipitate. It has been found that this excess water is released at 600°C.] Analysis by X-ray diffraction confirmed the material to be SnO_2 with possible Fe substitution into the lattice. Half of the batch is presently being heat-treated at 1100°C, after which the rest of the preparation and testing will be continued.

A problem is encountered with this method, however. The NH_4Cl which is sublimed is corrosive to the furnace and hood system. Some type of collection mechanism must be devised if this method is to be used. As an alternative, a batch is presently being prepared using NaOH as a substitute for NH_4OH. The NaCl thus formed should be easy to wash out with H_2O.

*Analyses by X-ray diffraction were done by B. Tani, Analytical Chemistry Laboratory, ANL.

C. Evaluation of Cathode Materials

1. Cathode Material Migration
(F. C. Mrazek and J. L. Smith)

The test apparatus for evaluating in-cell migration of cathode materials consists of 1.5-in. (38.1-mm)-diameter cells utilizing a conventional Ni/10% Cr anode, a hot-pressed tile as the electrolyte, and unsintered tapes of the chosen cathode material as the cathode. Two tape-cast materials,* NiO and Li_2MnO_3, were tested during this report period. Although NiO is not a new cathode material, it was included in this test program as a procedure check to be certain the deposition of metallic nickel observed in previous cells would be duplicated in this apparatus.

The heating cycle followed was to raise the temperature 20-30°C/h to 675 K and then from 675 to 925 K in two hours, where it remained for the duration of the 200-h test. This initial slow heating rate to 675 K is required for the removal of the organic materials present in the tape-cast cathodes. Gases to the cathode and anode consisted of 32.5% O_2-balance CO_2 and 80% H_2-balance CO_2, respectively, at flow rates of 50 cm^3/min. Both cells averaged 0.93 V over the entire 200-h test; (theoretical voltage for this gas combination is 1.08 V). Posttest disassembly of these cells suggests that this low voltage was due to poor wet seals.

Three 1-cm-long specimens of the electrolyte from each cell were examined microscopically. These samples were prepared and examined in the Inert Atmosphere Metallographic Facility. Examination by microscopy and scanning electron microscopy-energy dispersive spectroscopy (SEM-EDS) showed that the electrolyte in contact with the NiO cathode contained small particles of nickel (<1 to 5 μm) throughout the electrolyte thickness.

Microscopic examination and SEM-EDS of the electrolyte in contact with the Li_2MnO_3 cathode revealed no manganese-bearing precipitates.

A sample of the full thickness of each electrolyte was cleaned of any residual electrode material and submitted for chemical analysis. Each sample weighed ~0.5 g and had a cross-sectional area of ~1.7 cm^2. Table 1 presents the results of these analyses.

The manganese content in the electrolyte from the NiO-cathode cell may be thought of as the blank for the background manganese level for the electrolyte of the Li_2MnO_3 cell. The nickel content in the electrolyte of the NiO-cathode cell is equivalent to 8×10^{-7} mol Ni/cm^2, which is similar to results reported by G. Kucera.[2]

The apparatus has been modified to improve the wet seals, and additional tests are in progress.

*Supplied by T. Claar, Materials Science and Technology Division, ANL.

Table 1. Analyses of Electrolytes from Cathode Materials Migration Test

	Contaminants, ppm[a]			
	Mn	Ni	Fe	Cr
Electrolyte from NiO Cathode Cell	1.2	162	60	10
Electrolyte from Li_2MnO_3 Cathode Cell	10	18	120	38

[a]Analytical results by E. A. Huff, Analytical Chemist., Laboratory, ANL.

2. Cathode Material Solubility

(T. Kaun and T. Fannon*)

a. Cyclic Voltammetry

The solubility of lithiated NiO in a 75 mol % Li_2CO_3-K_2CO_3 melt was investigated by cyclic voltammetry. This technique has been described elsewhere.[3] Tests were conducted between 873 and 1023 K in a 1/3 O_2-2/3 CO_2 cathode gas environment. (This carbonate composition has an approximate 823-K liquidus.) Earlier examination of lithiated NiO solubility as a function of temperature indicated significant change in solubility due to the Li/K ratio of the carbonate melt. For the standard dry electrolyte composition of 62 mol % Li_2CO_3-K_2CO_3, NiO solubility increased from 5 to 45 wppm as temperature increased from 825 to 1023 K. In the presence of humidified 1/3 O_2-2/3 CO_2 gas, solubility as a function of temperature increased by nearly a factor of 10 and exhibited an irreversible increase in solubility of 2-4 times when returned to dry gas purge. In comparison, NiO solubility in 75 mol % Li_2CO_3-K_2CO_3 appeared to be <10 wppm for the temperature range 873 to 1023 K for the dry and posthumidified conditions. In tests with the purge gas humidified at room temperature, NiO solubility as a function of temperature increased in a range from about 20 wppm at 873 K to about 50 wppm at 1023 K. These initial results suggest that NiO stability under humid conditions is significantly improved with the higher Li_2CO_3 concentration electrolyte.

b. Pot-type Solubility Tests

A new pot-type solubility apparatus is now in operation; it includes improved purge gas/electrolyte contact and electrolyte circulation within the sample crucible. As illustrated in Fig. 8, each sample crucible contains a purge gas tube [3/16-in. (4.76-mm)-OD, 3/32-in. (2.38-mm)-ID, alumina] bubbling into the melt which is sheathed by a 1/4-in. (6.4-mm)-ID alumina tube. This arrangement provides an electrolyte circulating pump

*Student Researcher, Tennessee Technological University, Cookeville, TN.

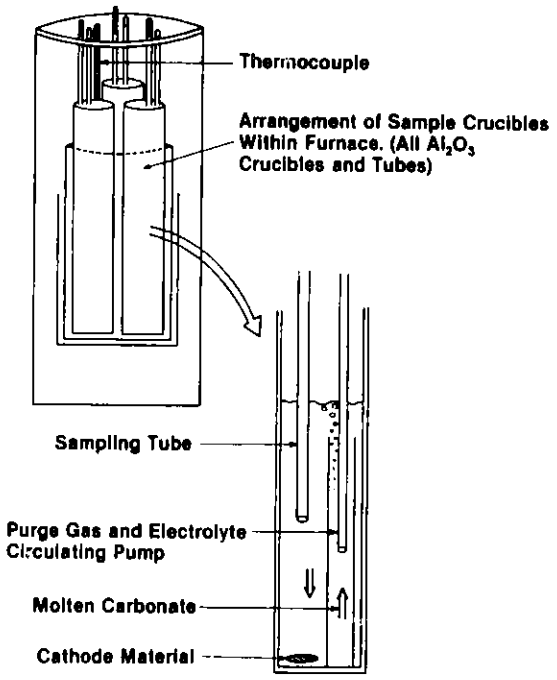

Fig. 8.

Arrangement of Pot-Type Solubility Apparatus. Operated at 823-1023 K with 30% CO_2-air atmosphere.

within the 60-cm^3 Al_2O_3 crucible. Equilibrium times are expected to be reduced in comparison to stagnant electrolyte tests, and temperature uniformity has improved with only a 10°C change from top to bottom of the 12-cm molten carbonate depth. In these experiments, solubility is determined from analysis of 1.0-g carbonate samples, which are periodically withdrawn from the sample crucible.

In the first round of experiments, the solubilities of NiO, $NiCoO_2$, and CoO in 62-mol % Li_2CO_3-K_2CO_3 or 38 mol % Li_2CO_3-K_2CO_3 at 823, 923, and 1023 K are examined. The samples are contained in 45 cm^3 of molten carbonate, which is exposed to 30% CO_2-air purge gas. The effect of humidification is also examined. We have recently introduced the capability of supplying 60°C (140°F) humidified cathode gas to our test apparatus. Each of the six purge lines is supplied with a heated water bubbler at a point just prior to entering the furnace. This was found to be satisfactory in reducing the amount of water condensing in the purge lines.

Future tests will examine solubilities of alternative cathode materials, i.e., ZnO, $LiFeO_2$, and Li_2MnO_3. This pot-type technique is intended to augment the cyclic voltammetric studies. We expect some of the materials to have potentials outside our working range with cyclic voltammetry.

3. Cell Testing
(J. L. Smith and J. R. Stapay)

Two cells, SQ37 and SQ38, were assembled this quarter for use in the examination of cathode dissolution/deposition phenomena. The first used a nickel oxide cathode and the second a tape-cast $LiFeO_2$ cathode.

The cell with the nickel oxide cathode (SQ37) incorporated a diffusion barrier of $LiAlO_2$ on the anode surface. This cell experienced two heater failures and was shut down at ~200-h running time. In posttest examination of the diffusion barrier, it appeared that the diffusion barrier may not have filled completely with electrolyte. Nickel deposits were seen in the usual area, the one third of the tile nearest the cathode.

Cell SQ38 was run to examine the migration phenomena associated with a $LiFeO_2$ cathode. The cell was assembled with a green tape of $LiFeO_2$. Due to a plumbing problem, the cell was inadvertently started without a fuel supply to the anode. No problems arising from this error were evident; however, the cell was shut down due to very poor open-circuit voltage. Disassembly and examination have not been completed, but it appears that the cathode may have shifted during assembly, resulting in a poor cathode wet seal.

D. Anode Development
(T. Kaun)

Recent evaluation of a foam metal structure (Retimet™) for application in MCFCs as an electrode/current collector/gas passage has spawned an approach for solving the problem of electrode creep or reduction of thickness in a MCFC stack under load over time. In addition to causing gas manifolding problems due to changing cell stack height, the shrinking electrode thickness, 1-2%, also degrades electrode performance by increasing contact resistances. Conventional components often are stacked as follows: high-surface-area electrode, current-collector, gas passage structure/bipolar plate (Fig. 9). Cell resistance increases due to corrosion and loss of contact between these members. Current work is aimed at reducing the electrode creep by the addition of ceramic particles to stabilize the high-surface-area structure to a creep resistance of 1-2% change in thickness.

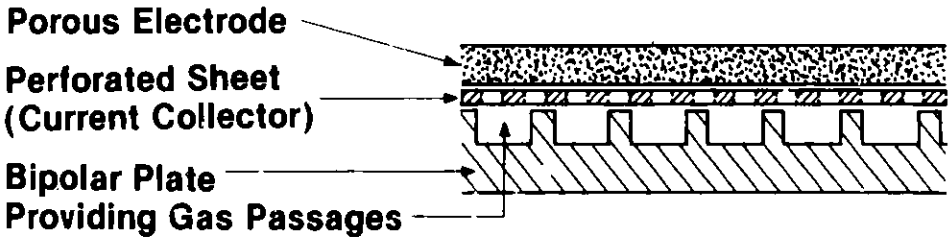

Fig. 9. Conventional MCFC Component Arrangement with the Electrode as a Load-Bearing Member

A factor-of-ten reduction in this degree of creep, to 0.1-0.2%, is expected by utilizing the foam metal structure (other structures such as conductive ceramic foams, honeycombs or "T"-folded perforated sheet could also be applied) as a superstructure, Fig. 10, with the electrode structure formed within it. Here, the electrode structure would be in intimate contact with its current collector, which also serves as the gas passage. A suggested method of fabrication is to press a tape-cast layer of powdered electrode

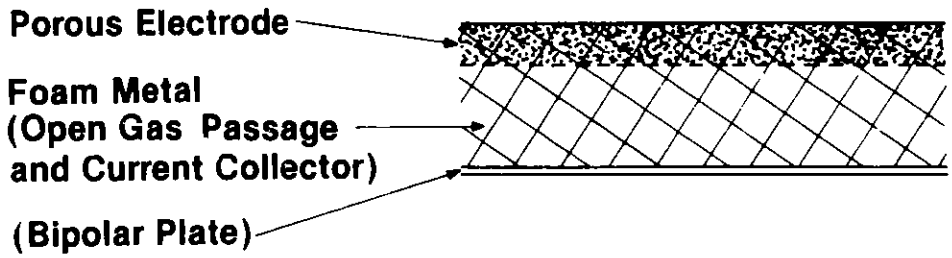

Fig. 10. Advanced MCFC Component Concept with the Electrode in a Superstructure to Bear Compression Loading. Mechanical creep is reduced by at least a magnitude from 2% to 0.1% thickness change.

material onto the foam metal structure before sintering. Also, roll-pressing the electrode structure (Gould, sintered nickel electrode) into the foam structure has provided desired results. Another advanced feature has also been introduced. The bi-polar plate has been intimately attached to the Ni-Cr foam metal by furnace brazing. This integrated anode structure should decrease the possibility of increased contact resistance due to loss of stack compression or corrosion.

With a superstructure as support, therefore, the electrode is not required to bear load and tolerates electrode sintering without impacting the overall cell stack dimensions. The electrode also has improved current collection without reduced electrode face exposure. (A metal separator formed to provide flow channels, with or without a perforated sheet current collector, can partially mask the electrode face.) The superstructure design should improve MCFC performance as well as alleviate design problems. The foam support structure also provides a convenient site for reforming catalyst in the development of a MCFC designed to provide internal reforming.

Samples of this integrated electrode/current-collector have been fabricated using a number of approaches. These samples are being evaluated metallographically.

E. Ceramic Materials Development

(R. B. Poeppel,* T. D. Claar,* R. J. Fousek,* J. J. Picciolo,* and D. Pickrell†)

1. Fabrication of Cathode Structures

Experiments have been performed to determine the sintering conditions suitable for fabricating porous pellets of alternative cathode materials for use in stability testing. Powders of $LiFeO_2$ and Li_2MnO_3 were dispersed in methylene chloride, using 5 wt % Acryloid B-72™ as a binder.

---

*Materials Science and Technology Division, ANL.

†Undergraduate Research Participant from Ohio State University, Columbus, OH.

After the solvent was evaporated, the powders were screened to -60 mesh and cold-pressed into cylindrical pellets 0.5 in. (1.27 cm) in diameter. Pellets of each material were then sintered in air at 900°C for 1 h and at 1200°C for 15 min. The results from these tests, presented in Table 2, indicate that pellets of ~40% porosity can be obtained by sintering $LiFeO_2$ at 900°C and Li_2MnO_3 at 1200°C. The Li_2MnO_3 pellets exhibited essentially no densification at either temperature, but the 1200°C sintering produced a much stronger pellet than the 900°C treatment. Additional pellets of these materials of ~60% T.D. (theoretical density) will be prepared for stability testing, and the effort will be expanded to include ZnO materials.

2. Electrolyte Matrix Fabrication Studies

The objective of this activity is the fabrication of thin [0.02-0.03 in., (0.51-0.76 mm)] ceramic electrolyte matrices for cell testing under other tasks in the program. Current efforts are focusing on γ-$LiAlO_2$ electrolyte support materials either synthesized in-house using a spray-drying process or obtained from commercial suppliers. Matrices will be fabricated by tape-casting and powder-rolling processes.

Table 2. Results of Alternative Cathode Sintering Tests

Pellet No.	Material	Forming Pressure, psi (MPa)	Green Density,[a] g/cm^3	Sintering Conditions	Fired Density g/cm^3	Fired Density % T.D.[b]
F2	$LiFeO_2$	10,186 (70.2)	2.45	1200°C/15 min	3.16	71.3
F3	$LiFeO_2$	15,279 (105.3)	2.55	900°C/1 h	2.58	58.2
M2	Li_2MnO_3	10,186 (70.2)	2.26	1200°C/15 min	2.31	60.8
M3	Li_2MnO_3	15,297 (105.3)	2.39	900°C/1 h	2.32	61.1

[a]Corrected for binder content.

[b]Based on theoretical densities of 3.80 g/cm^3 for Li_2MnO_3 and 4.43 g/cm^3 for $LiFeO_2$.

A batch (No. 207-58-600) of predominantly β-$LiAlO_2$ powder (~150 g) has been obtained from J. Sim of ANL-CMT. This material was prepared by spray drying an aqueous slurry of $Al(OH)_3$ and $LiOH \cdot H_2O$ and firing at 600°C for 3 h.[4] (In an earlier study by J. Sim,[5] powders of this type were tape-cast, then simultaneously sintered and converted to γ-$LiAlO_2$.) Approximately 100 g of the β-$LiAlO_2$ powder has been further calcined at 900°C for 1 h to convert the $LiAlO_2$ to the γ-phase, which is more stable in the cell environment, and to reduce the surface area from ~20-25 m^2/g to 14 m^2/g, as determined by B.E.T. analysis. Analysis by X-ray diffraction indicated γ-$LiAlO_2$ as the major phase in the calcined product, with a very-very minor amount of

α-$LiAlO_2$. Scanning electron microscopy of the 900°C calcined material revealed roughly spherical agglomerates (2 to 15-μm-dia) of submicron-sized crystallites.

A series of experimental $LiAlO_2$ tape matrices was prepared by tape casting of the spray-dried lithium aluminate material. The general procedures consisted of dispersing the $LiAlO_2$ powder into a solvent to form a slip, using Grade Z-3 Menhaden fish oil as a deflocculant. After the suspension was ball-milled overnight, the appropriate binders and plasticizers were added, and the slip was mixed on the ball mill for several additional hours. The slip was then agitated in an ultrasonic bath and partially evacuated to remove entrained air bubbles. Tapes were formed by casting the slip onto Teflon sheets and using a moving doctor blade to prepare the desired casting thickness. The formulations of the $LiAlO_2$ slips are summarized in Table 3.

Table 3. Summary of $LiAlO_2$ Tape-Casting Trials

Slip No.	Composition	Casting Thickness	Comments
LA-1	32.0 g $LiAlO_2$ (600°C)[a] 60.5 g Cerbind 73151	A - 40 mils B - 20 mils	Tape A developed numerous drying cracks; Tape B was free of cracks.
LA-2	62.0 g $LiAlO_2$ (900°C)[a] 1.25 g Z-3 fish oil 83.5 g solvent[b] 9.0 g PX 316 11.1 g UCON-50-HB-2000 11.0 g B-98 PVB	A - 30 mils B - 40 mils C - 40 mils	Slip viscosity ≈ 1000 cP Minor cracking of dried tape.
LA-3	24.0 g $LiAlO_2$ (900°C)[a] 0.6 g Z-3 fish oil 30.2 g solvent[b] 2.85 g PX 316 5.85 g UCON-50-HB-2000 4.0 B-98 PVB	A - 50 mils	Slip viscosity ≈ 3100 cP Minor cracking of dried tape.
LA-4	23.0 g $LiAlO_2$ (900°C)[a] 30.1 g isopropyl alcohol 0.4 g Z-3 fish oil 60.0 g Cerbind 73200	A - 20 mils B - 40 mils C - 40 mils	Slip viscosity ≈ 1700 cP No cracking problems. Minor surface roughness.

[a]Temperature at which γ-$LiAlO_2$ was calcined.

[b]58 vol % xylene - 42 vol % ethanol.

Slip LA-1 was prepared from the relatively high-surface-area spray-dried β-$LiAlO_2$ fired at 600°C, using an acrylic binder system and methyl chloroform-methylene chloride solvent. Tapes were cast at thicknesses of 20 and 40 mils; the dried tapes were approximately 6.5 and 14 mils thick, respectively. The tape cast at 20 mils was generally free of cracks, while the thicker tape cast at 40 mils developed many shrinkage cracks during drying.

Slip LA-2 was formulated from the γ-$LiAlO_2$ powder calcined at 900°C, using solvent, binder, and plasticizer materials investigated previously under this program for tape casting of β-$LiAlO_2$.[4] Tapes cast with doctor blade settings of 30 and 40 mils dried to thicknesses of approximately 11 and 16 mils, respectively. A few minor cracks were observed in these tapes, although they were much less significant than those that formed in the 40-mil tape cast from slip LA-1. Crack-free tapes approximately 4.5 x 4.5 in. (11.4 x 11.4 cm) in area were cut from the LA-2 series tapes.

Slip LA-3 was a formulation similar to that of LA-2, and again utilized the γ-$LiAlO_2$ powder calcined at 900°C. A tape cast at a blade setting of 50 mils dried to a thickness of ~23 mils. A few cracks developed in this tape, and several isolated areas of the tape appeared to contain inadequately dispersed $LiAlO_2$ agglomerates.

Slip LA-4 was prepared by dispersing spray-dried γ-$LiAlO_2$ in isopropyl alcohol and adding a vinyl binder (Cladan Cerbind 73200) after ball milling overnight. A tape cast at a 20-mil setting dried to a thickness of ~6 mils, while those cast at a 40-mil setting dried to thicknesses of ~8 to 10 mils. The tapes were very strong, and no cracking occurred. However, the top surfaces were slightly textured, possibly as a result of inadequate dispersion of the $LiAlO_2$ agglomerates.

Specimens will be cut from the various $LiAlO_2$ tapes for organic burnout and characterization of green density and microstructure. In future tape-casting experiments, several alternative techniques will be evaluated for more effectively dispersing the ceramic particles in the slip. A vibratory mill, ultrasonic disperser, and high-shear mixer have been ordered for this purpose.

A new batch of spray-dried $LiAlO_2$ has been prepared for the electrolyte matrix fabrication studies. Batch SLA-1 was processed by spray drying a slurry consisting of 305.0 g $Al(OH)_3$ (Alcoa H710) and 162.1 g $LiOH \cdot H_2O$ in 3 L of deionized water. The spray-dried powder was further processed by calcining 20 h at 600°C and 1 h at 900°C. Characterizations of the final $LiAlO_2$ product are in progress.

Efforts are also in progress to investigate the feasibility of forming acceptable electrolyte matrices from commercially available $LiAlO_2$ powders. Lithium aluminate materials have been received from Lithco and Alfa Ventron for evaluation. Analyses by X-ray diffraction indicate that both commercial materials are predominantly γ-phase $LiAlO_2$ with very minor to minor amounts of α-phase. Scanning electron microscopy of the as-received $LiAlO_2$ materials revealed that both materials consist of agglomerates. The Lithco material contains agglomerates ranging in size from ~10 to 200 μm, although the larger agglomerates could be broken up by ultrasonic agitation. These smaller agglomerates were composed of $LiAlO_2$ crystallites ~0.5 to 3 μm in size. The Alfa-Ventron powder consists of agglomerates ~100 to 200 μm in size, which could not be broken up by ultrasonic agitation. These agglomerates consisted of thin plate-like crystals of $LiAlO_2$ several microns across the face and ~0.1 to 0.2 μm thick. Scanning electron micrographs of these two materials are compared in Figs. 11 and 12. The B.E.T. analyses indicate that the Lithco material has a surface area of 1.6 m^2/g, while the Alfa $LiAlO_2$ powder has a surface area of 3.3 m^2/g.

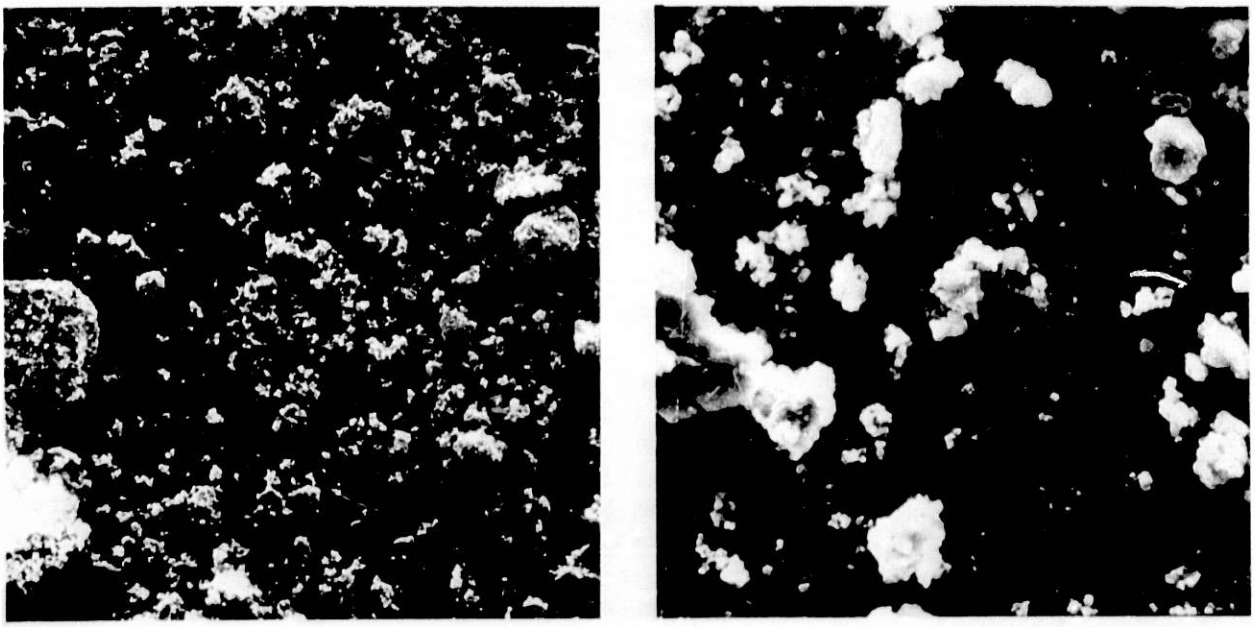

a b

Fig. 11. Scanning Electron Micrographs of Lithco γ-$LiAlO_2$ (Lot No. 421-82-11-1)

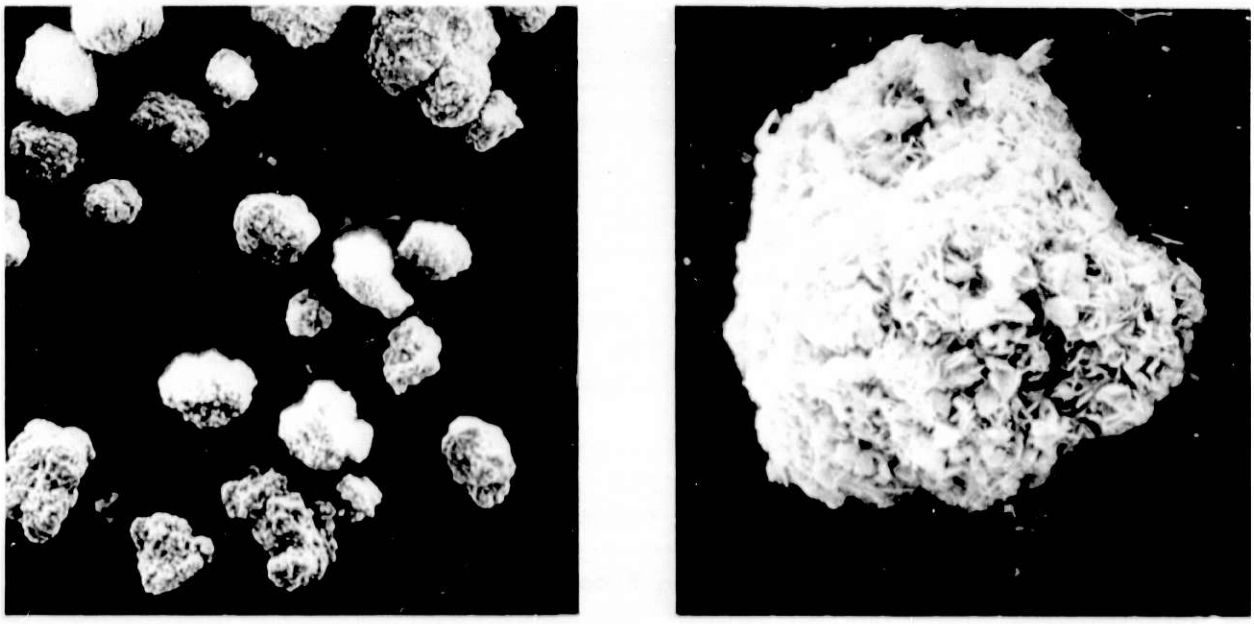

a b

Fig. 12. Scanning Electron Micrographs of Alfa Ventron γ-$LiAlO_2$ (Lot No. 111979)

Five-pound samples of the Lithco $LiAlO_2$ material have been sent to outside vendors for comparison of their capabilities to jet mill the powder to the submicron particle sizes required for the matrix. The jet-milling equipment under evaluation includes: the Donaldson Mini-Grinder in series with the Model A-12 Classifier, the Trost TX Laboratory Mill, the Sturtevant 4-Inch Micronizer Mill, and the Fluid Energy Model 2-Inch Micro-Jet System. Each vendor is attempting to mill the powder to a mean particle size in the range of 0.3 to 0.5 μm. The milled powders will be characterized by scanning electron microscopy, B.E.T. surface area, and particle size distribution, and will be utilized in the matrix fabrication studies.

Work has also been initiated on the evaluation of powder rolling as an alternative process for fabricating thin $LiAlO_2$ matrices. The initial efforts are focusing on the use of polyisobutylene (PIB)* as the binder and plasticizer, and Lithco $LiAlO_2$ jet-milled in the Trost TX Laboratory Mill. Several formulations, containing from 10 to 20 vol % PIB, have been prepared by dissolving the PIB in toluene, dispersing the $LiAlO_2$ powder to form a thin paste, and then evaporating the toluene while stirring (see Table 4). The dried powder cake was then pulverized with a mortar and pestle and screened to -30 mesh. The screened powders were then cold-pressed in a steel die at pressures of ~10,000 psi (68.9 MPa) to form compacts approximately 2.2 in. × 2.2 in. × 0.3 in. (5.6 cm × 5.6 cm × 0.76 cm), which will subsequently be rolled into thin sheets approximately 0.02 in. (0.51 mm) thick. This powder-rolling operation will be performed in the Materials Processing and Development Group of MST during the next reporting period.

Table 4. Formulation of $LiAlO_2$[a]/Polyisobutylene (PIB) Mixtures for Powder-Rolling Experiments

Mixture No.	Composition	PIB Content, vol %
LAP-8	100 g $LiAlO_2$ 8.9 g PIB 160 g toluene	20
LAP-9	100 g $LiAlO_2$ 6.9 g PIB 160 g toluene	15
LAP-10	100 g $LiAlO_2$ 4.0 g PIB 160 g toluene	10

[a]Lithco $LiAlO_2$ jet-milled in Trost TX Laboratory Mill.

*Vistanex LM Polyisobutylene, Exxon Chemical Co., Houston, TX.

F. MCFC Systems Code
(S. A. Zwick)

Members of the Fuel Cell Office use the SALT system code to analyze MCFC power plants. Considerable analysis has been carried out for methane-fueled plants. Internal methane reforming ($CH_4 + 2H_2O \rightarrow CO_2 + 4H_2$) is particularly attractive since it reacts exhaust H_2O with methane fuel and, being an endothermic reaction, absorbs heat directly from the cells. Unfortunately, the reforming calculations in SALT's chemistry routine PROP converge very slowly to equilibrium solutions in some cases, causing the corresponding plant runs to halt. This happens when only a small amount of methane is present at equilibrium and/or when the standard starting estimates in PROP are far from the correct solutions.

1. Adaptation of the CHEQ Routine for Initial Guesses

A way of starting PROP equilibrium calculations would be to divide the total space of solutions into regions in which only certain known species were dominant. In the case of PROP, with 21 active species composed of the six elements--C, H, K, N, O, and S, plus Ar--this would be a prohibitive task. For temperature, pressure, and chemistry ranges apt to occur in fuel cell plants, however, C, H, and O-reactions involving only six active species--CO, CO_2, CH_4, H_2, H_2O, and O_2, plus N_2--are likely to dominate. The solution space reduces to a two-dimensional C, H, O-phase diagram, and the breakdown into dominance regions is not difficult to carry out. Roughly, the dominance regions correspond to reforming (CH_4, H_2, and CO), shift (CO, CO_2, H_2, H_2O), excess O_2 (CO_2, H_2O, O_2), and carbon deposition zones. These zones change character at about 900 K (critical for the reforming reaction).

The CHEQ routine now under development for the fuel cell solid oxide code computes equilibrium for the six species listed in the paragraph above, and also for CH_3OH (unstable, but possible), using the dominance zones indicated there. The CHEQ routine performs sufficiently well at this time to serve as a device for starting out the PROP runs. Therefore, the current version was transcribed from Fortran IV to PL/I and installed in SALT, where it can be called as a user option to start PROP runs. In runs which PROP previously could not handle, the use of CHEQ reduced the number of iterations from over 100 (PROP limit), to convergence at 40 iterations (a typical PROP calculation value), when PROP's search and convergence controls--which failed in this case--were suppressed.

With respect to the conversion of CHEQ to PL/I, it turns out that while the CMS system on which SALT operates is capable, in principle, of combining Fortran routines with PL/I main programs, it actually requires extensive revisions in the PL/I codes to work. These have to do with differences in the way PL/I and Fortran store data in memory and pass arguments to subroutines. Also, the operating system must start programs with Fortran routines rather than PL/I codes, unless the load procedure is adjusted. It proved simpler to rewrite CHEQ in PL/I than to modify SALT for the Fortran routine, and the approach used also makes installing user controls much easier.

2. PROP Search and Convergence Updates

With good estimates of gas compositions being fed to PROP from CHEQ, the ball-park search method in PROP had to be reduced. This procedure steps the principal PROP variables, y (an atomic oxygen parameter) and z (an atomic hydrogen argument), by factors of 10^6 until the solutions are exceeded, then reduces them to 10^3 and reverses the step directions, etc. To accommodate CHEQ, the steps are started from a factor of 2. In addition, search step size reductions beyond this point were changed to powers of 0.8 instead of square roots of the step ratio (which tended to stall the search). The search stops at 5% steps in x or y. With these changes, PROP converged in about five steps more than with no search. However, it seems risky to back off the search any further. (The user can eliminate the search in any given case.)

PROP iterations will always converge if no search or convergence techniques are used, although, for reforming calculations that failed, several hundred iterations would have been required. To speed convergence, a technique that involved y and z separately was originally written into PROP. This failed for the reforming and other problems and was bypassed for general use. A simpler, successive over-relaxation (SOR) method, which adds in each iteration some factor times the change in y and z, was found to work well with both CHEQ and PROP and has been installed. The SOR method reduced convergence times by about 20% for the reforming problem.

3. User Controls

Some new parameters were written into SALT to allow users to decide whether the latest changes should be kept or bypassed. These can be set by the usual SALT method of writing lines of PLI (such as: FROZEN = 0;) into the struct file for a plant. A partial list of controls is given in Table 5 below.

Table 5. SALT User Parameters

(Type, Range)	Name	Parameter Controls[a]	New Preset to
(Intg, 0 to 2)	Switch0:	Which property routine is used. (0-TPRSP, 1-PRONEW, 2-PROP)	2
(Intg, 0 or 1)	Switch1:	Whether CHEQ is called (1) or not (0).	0
(Intg, 0 to 1)	Srch:	Use PROP search (1) or not (0).	1
(Real, 0. or 1.)	Cvge:	PROP SOR constant; use 0. to omit.	.35
(Intg, -4 to 2)	Iprop:	PROP diagnostic printouts; use 0 to omit.	0
(Intg, 0 or 2)	Icheq:	CHEQ diagnostic printouts; use 0 to omit.	0
(Intg, 0 to 1)	Frozen:	Chemistry active (0), or all inert (1).	0
(Real, 0. to 1.)	Inert:	Separate species controls, if Frozen is 0. (Inert.CH4 = .5 makes CH4 'half inert'.)	0., except for Inert.H2OL = 1
(Real, in dg K)	T_lower:	Active species are inert below T_lower, active above T_upper, graded between.	1.
(Real, in dg K)	T_upper:		0.
(Real, in dg K)	Tmin(22):	Separate species (1 to 22) controls, if T_upper is set less than T_lower.	1.
(Real, in dg K)	Tmax(22):		0.

[a]Currently, CHEQ will not respond to the inert controls (except that if Frozen = 0, neither PROP nor CHEQ will be called).

III. ADVANCED CONCEPT FOR SOLID OXIDE FUEL CELLS

A. Background

A new fuel cell technology is being developed at CMT. This new design concept, called the monolithic fuel cell, will have roughly 100 times the power density of conventional fuel cells. The stack design employs the thin ceramic-layer components of existing solid oxide fuel cells in a strong, lightweight, honeycomb structure of small cells, and thus achieves unequaled power per unit mass or volume. A monolithic fuel cell would convert hydrocarbon fuel to dc power at 50% efficiency, which is higher than other technologies that use this fuel.

In the monolithic concept, fuel and air are combined electrochemically in a ceramic cell at an operating temperature of 1100 tc 1300 K. Cell components are fabricated as one piece, much like a block of corrugated paperboard. Fuel and oxidant are conducted through alternating passages in the stack, as shown in Fig. 13. These passages are formed from thin (25 to 100 μm) layers of the active cell components: the anode, cathode, electrolyte, and the interconnection material that connects cells in electrical series (bipolar plate). The corrugations also form the gas seal at the edges of the structure. Advantage is taken of the ability to fabricate the solid electrolyte and other solid cell components into shapes that cannot be achieved in liquid electrolyte systems. In liquid electrolyte systems, much of the mass and volume goes into building the inert container for the liquid. Eliminating this unnecessary material helps give the monolithic fuel cell a significant advantage in performance.

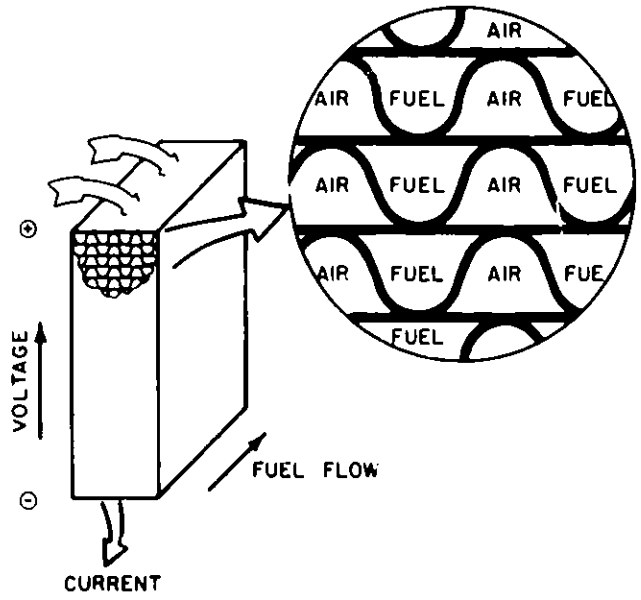

Fig. 13.

Monolithic Fuel Cell

The high power density of the monolithic fuel cell results from the small cell size. Cells with gas passages 1 to 2 mm in diameter or smaller are achievable when the inert container for electrolyte and the inert support for the thin active layers are eliminated. The small cell size increases the active surface area per unit volume of the cell. For example, a monolithic

cell stack with gas flow channels of about 2-mm dia has an active-surface to cell-volume ratio of 10 cm^2/cm^3, compared to 1 to 2 cm^2/cm^3 for conventional fuel cells (phosphoric acid, molten carbonate, solid oxide), as shown in Fig. 14. This reduces the volume of the fuel cell stack by a factor of five or more; larger reductions in volume are achieved with gas flow channels even smaller than 2 mm. However, the resistance to gas flow also increases as the size of the gas passage is reduced. Gas flow resistance depends somewhat on the overall manifolding and generator design, which have yet to be optimized for a monolithic fuel cell system. Nevertheless, gas flow channels of 1- to 2-mm diameter appear feasible, based on operating experience in other systems.

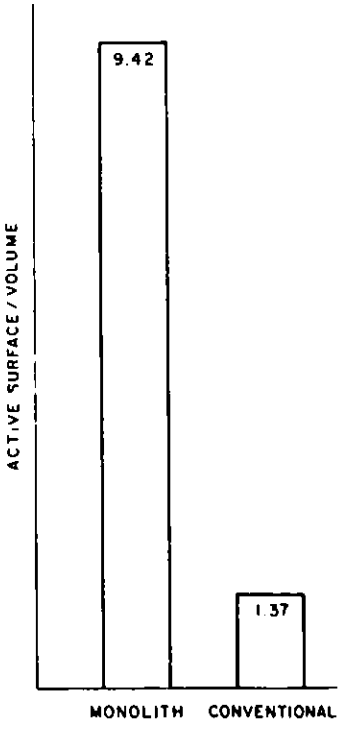

Fig. 14.

Comparison of Monolithic and Conventional Fuel Cells

More important, the small cell size in the monolithic design reduces the voltage losses due to internal electrical resistance. This reduction is an important consideration, because internal resistance is the principal dissipative loss for the ceramic materials and temperatures of interest. Decreasing the cell size decreases the current path length because current is carried "in-plane" by the electrodes in the monolithic design. As shown in Fig. 15, electrons (coming from the adjoining cell in electrical series) flow through the plane of the interconnection, then partway around the circumference of the air passage in the plane of the air electrode. At the air electrode/electrolyte interface, the electrons are consumed in the formation of oxide ions, which are transported through the plane of the electrolyte. At the fuel electrode/electrolyte interface, the reaction of hydrogen with the oxide ions forms water. The released electrons flow partway around the circumference of the fuel passage in the plane of the fuel electrode, then

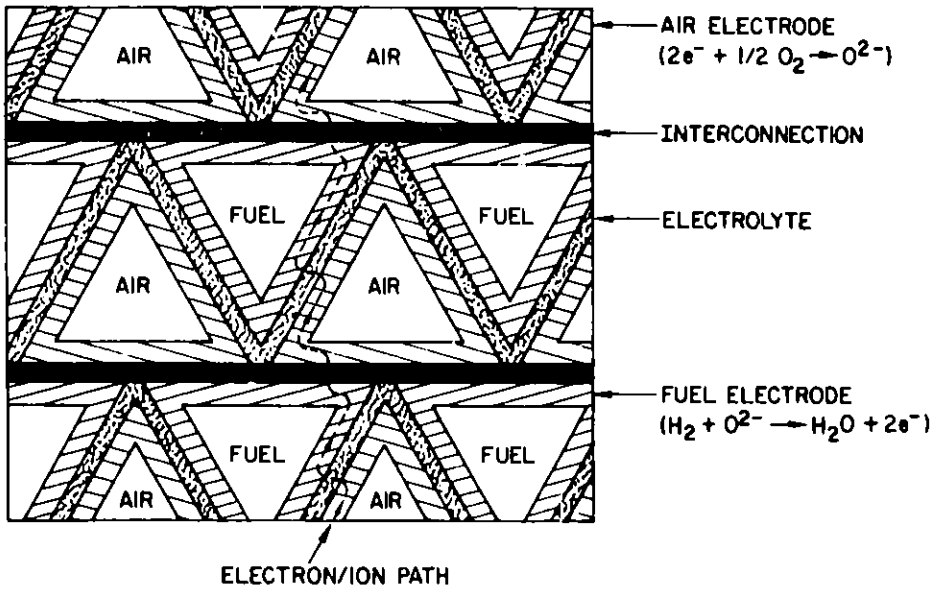

Fig. 15. Current Flow Path in Monolithic Fuel Cell

through the plane of the interconnection into the next cell in electrical series. The small cell size (i.e., the small distance between interconnection layers) decreases the current path length in the electrodes and reduces the voltage losses due to internal resistance, as compared to conventional fuel cells in Fig. 16. As a result, monolithic cells can be operated at higher current densities than conventional cells, yet achieve the same output voltage.

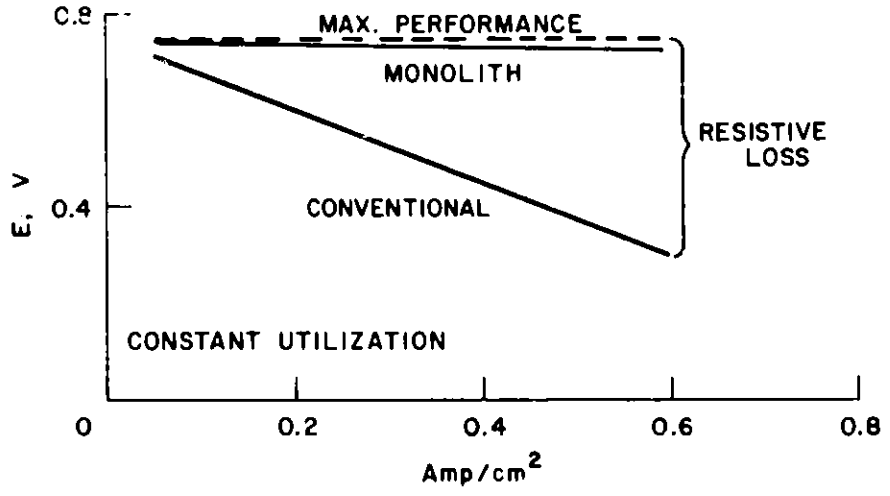

Fig. 16. Resistive Losses in Monolithic and Conventional Fuel Cells

The high current density of the monolithic fuel cell results from the small cell size and correspondingly low internal resistance. As a consequence of the low internal cell resistance, the current density is high at the fuel inlet (and low at the fuel outlet) of the fuel channel, as shown in Fig. 17. The low current density at the fuel outlet is desirable because overall cell performance is determined by the voltage losses due to internal resistance at the cell outlet. (Voltage losses arising from resistance to gas phase diffusion are negligible due to the thin electrodes.) Small resistance polarization losses (1 to 5 mV) at the fuel outlet mean that the fuel electrode, as an equipotential surface, approaches the maximum theoretical voltage (Nernst potential) set by thermodynamic considerations. The optimum cell performance is obtained when the average current density is increased to the point where resistance polarization losses at the fuel outlet just become significant, as shown by the dashed curve in Fig. 17. As a result, the cell nearly always operates within a percent or so of the maximum efficiency, even at high power output.

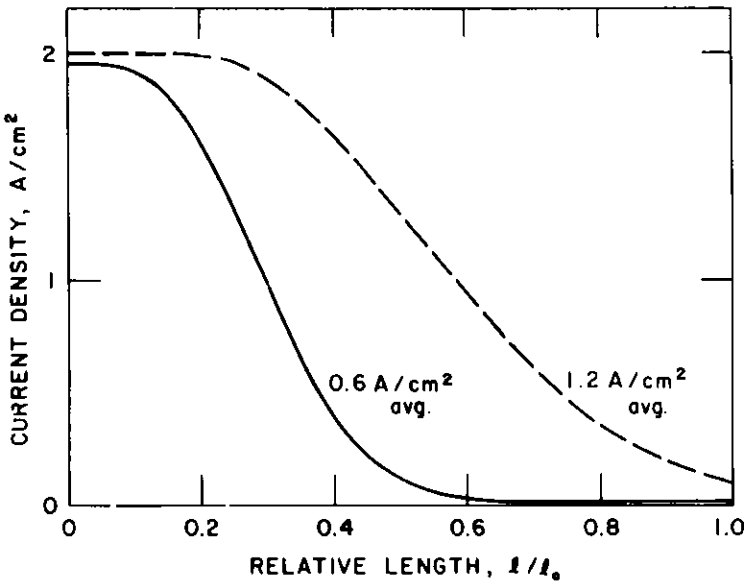

Fig. 17. Axial Current Distribution along Fuel Channel. Fuel enters at relative length of 0 and exits at relative length 1.0.

Monolithic fuel cell stacks will have high power per unit volume, as shown in Fig. 18. Further, monolithic fuel cell stacks will have high power densities, as shown in Fig. 19, as a result of the high active surface area, high current density, and low weight. The low weight results chiefly from the elimination of inert materials to contain the electrolyte or support the thin active layers. In the monolithic design, the thin ceramic layers are self-supporting over the small distances involved. An additional weight reduction comes about from the thin electrodes, which are possible due to the short current paths. Again, there is a benefit of the reduced cell size. The increase in power density accruing from the small cell size is the major incentive for adopting the monolithic cell approach.

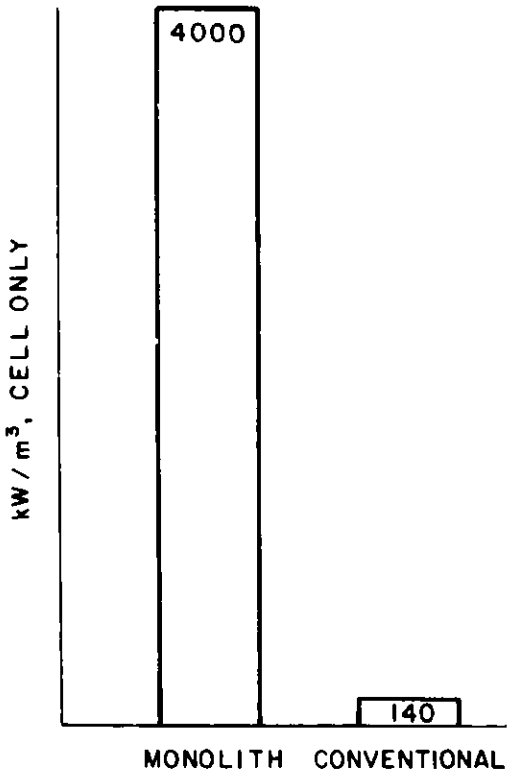

Fig. 18.

Volumetric Power Density

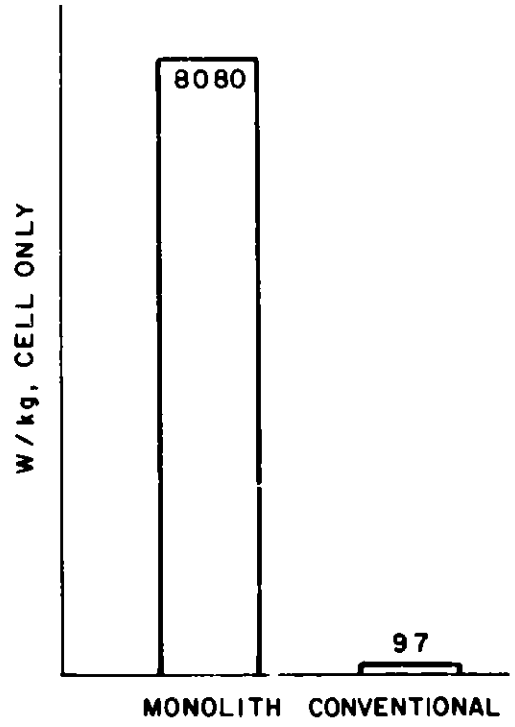

Fig. 19.

Power Density of Active Fuel Cell Area (excluding manifolds and insulation)

B. Advanced Fabrication

1. Electrolyte Fabrication

(R. K. Steunenberg, P. E. Papierski,* and F. C. Mrazek)

The electrolyte fabrication effort was focused on the development of a tape-casting procedure for the fabrication of of Y_2O_3-stabilized ZrO_2 electrolyte. Zircar Type ZYP ZrO_2, which is stabilized with 16.9 wt % Y_2O_3, was selected for these studies on the basis of its small particle size (<0.1 μm) and large surface area (44 m^2/g), which result in very good sintering characteristics.[6,7] The Cladan binder system No. 73200 (Cladan Technology Inc.), which consists of a vinyl binder dissolved in isopropanol, was used to prepare a series of slips for tape casting. A few preliminary experiments with this system had shown that it has certain favorable properties in that the tapes do not tend to adhere to themselves and are not hygroscopic. However, the tendency of the Zircar material to form agglomerates presented some difficulties. In addition, the tapes were weak and tended to tear due to shrinkage during drying. Because of these problems, the immediate effort was directed toward a means of improving the quality of the green tapes.

For the 73200 binder system, Cladan recommends a solids:solvent:binder weight ratio of 3:1:2. Several experiments were performed, using this basic system with various modifications, in an attempt to reduce or eliminate the agglomeration effects observed earlier. A small amount of slip was prepared using an ultrasonic treatment with a Sonicator Model 10 Cell Disrupter, rather than the usual ball-milling procedure, to disperse the ZrO_2 in the solvent and to mix the resulting dispersion with the binder. A green tape cast from this material was of low strength and showed extensive agglomeration of the ZrO_2. A separate test in which the ZrO_2 was exposed to 20 min of ultrasonic treatment in isopropanol showed some reduction in the size of the agglomerates, but very little overall improvement.

Since it was suspected that the Burundum (Al_2O_3) 0.5-in. (12.7-mm)-dia cylinders normally used for ball milling were relatively ineffective because of the viscosity of the slip material, a slip was prepared in which all of the ball-milling operations were performed with 0.5-in. (12.7-mm)-dia steel balls. The green tape resulting from this material was of slightly better quality, but agglomerates up to 0.4 mm in diameter were present. A similar slip was prepared, by ball milling for 2.3 h with Burundum cylinders, in which 1.4 wt % corn oil was added to the mixture as a deflocculant. The corn oil appeared to have little or no effect in reducing the degree of agglomeration. An additional slip was prepared by 20 h of ball milling, in which 0.8 wt % Type Z-3 Menhaden fish oil was added as a possible deflocculant. A tape that was cast from this slip showed that the fish oil was also ineffective in reducing the size or number of agglomerates. A series of settling experiments in which the as-received Zircar ZrO_2 was added to isopropanol containing increasing concentrations of the fish oil showed that the oil actually decreased the stability of the dispersions, as indicated by higher settling rates.

---

*Resident Student Associate, Univ. of Illinois Medical School, Chicago, IL.

At the suggestion of Prof. R. Buchanan of the University of Illinois (Champaign), the addition of water to the isopropanol solvent was investigated. Preliminary tests indicated that the agglomerates were almost entirely dispersed by a 30-min exposure to the ultrasonic probe in water, whereas this treatment had essentially no effect in isopropanol. A subsequent set of similar tests with isopropanol-water solutions containing increasing concentrations of isopropanol indicated that good dispersion of the agglomerates occurred at isopropanol concentrations up to about 60 wt %. A slip was prepared, using equal weights of 60 wt % isopropanol-40 wt % water solvent and ZrO_2 powder, followed by the addition of Cladan No. 73200 binder in the usual 2:3 weight ratio of binder to ZrO_2 powder. During the ball-milling operation with Burundum cylinders, it was clear that the milling action was much improved over that for the previous slips. Tapes cast from this slip showed essentially no agglomeration at 10 X magnification, as opposed to those prepared previously with the isopropanol solvent (see Fig. 20). Otherwise, the quality of the tapes was comparable to that of those prepared earlier.

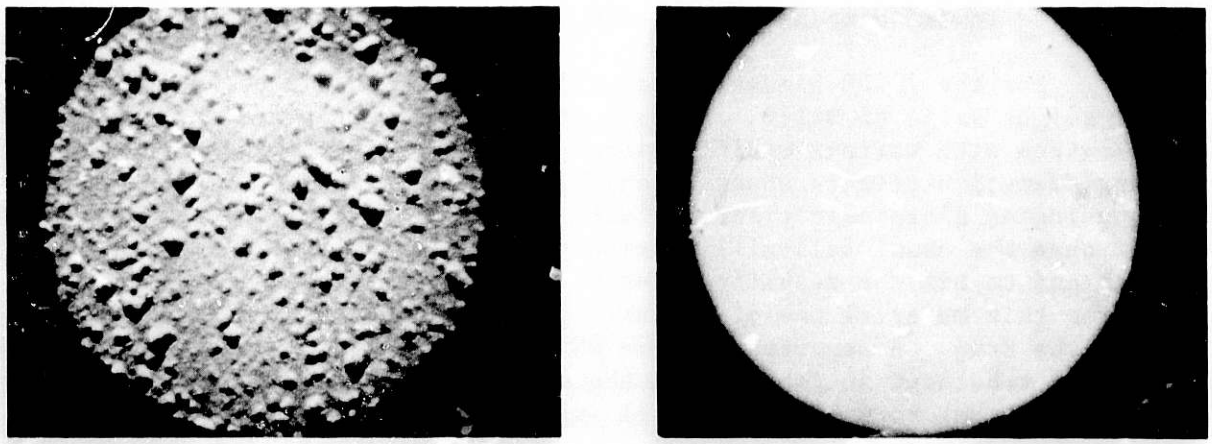

a. Solvent: Isopropanol

b. Solvent: 60 wt % Isopropanol 40 wt % Water

Fig. 20. Effect of Solvent on Agglomeration of Y_2O_3-Stabilized ZrO_2. (Green tapes prepared from Zircar Type ZYP Zirconia and Cladan No. 73200 Cerbind System.)

During these studies, samples of the materials were taken throughout the various steps of slip preparation, spread on microscope slides, and allowed to dry. Examination of these samples showed that agglomerates of about the same size were present in all steps of the process, including the starting material. Ball milling, ultrasonic agitation, and the use of oil deflocculants were ineffective when used with the isopropanol solvent alone. The addition of water to this particular ZrO_2-solvent-binder system, however, appears to be highly effective in reducing the extent of agglomeration. The reason for this behavior is not yet known, but it may be related to surface-tension effects (better wetting and penetration by the water), the more polar nature of water, or possibly to the tendency of the water to remove chloride impurities from the ZrO_2.

The Y_2O_3-stabilized ZrO_2 used in these studies is known to contain about 0.8 wt % chloride as an impurity, and the chloride content has been observed to be higher in the larger particles.[8] This observation suggests that removal of the chloride may result in a smaller, more uniform particle size that should provide a higher density of ZrO_2 in the green sheet and enhance the density of the final sintered sheet. It has also been reported[9] that the presence of the chloride raises the required sintering temperature of the material by as much as 150°C, in order to achieve high density.

A "laundering" procedure for the removal of chloride from the ZrO_2 has been reported by Scott and Reed.[6,9] This procedure involves repeated washing of the ZrO_2 with water, followed by centrifugation and removal of the supernatant water after each washing step. In the washing step, the solids content of the suspension is <1.0 wt %, which requires large volumes of the suspension in the centrifugation step. An attempt is being made to modify the procedure to accommodate a higher solids content of about 5 wt %. The proposed modifications include the addition of ultrasonic agitation and heating of the suspension in each washing step to facilitate the removal of chloride from the ZrO_2. One small batch of ZrO_2 has been treated according to the modified procedure; the results will be available when chloride analyses of the wash solutions have been completed.

2. Electrolyte Sintering Studies
(J. W. Sim)

The near-term objective of this work is to define the experimental conditions required to provide a thin sheet [~0.001-in. (0.025-mm) thick] of high-density (>95%) Y_2O_3-stabilized ZrO_2. The longer-term objective is to produce a composite structure containing one or more porous electrode layers and a dense Y_2O_3-stabilized ZrO_2 electrolyte layer. The effort focuses on tape casting and sintering. Each step in the fabrication process is briefly discussed.

a. Powder Considerations

The powder used in these experiments is the Y_2O_3-stabilized ZrO_2 (16 wt % Y_2O_3) produced by Zircar, Inc., Florida, NY. This powder has a very high surface area (44 m^2/g), and consequently it sinters well. The sintering behavior of Zircar powder is reported in the literature.[6,7] Chloride ion, which is present at levels of 0.8 wt %, affects the sintering kinetics at sintering temperatures of less than 1350°C, but it does not affect sintering at higher temperatures.[6] Thus, if sintering is to be performed at ≤1350°C, the powder should be washed to remove the chloride. A method of washing the powder is described in the literature.[9] Calcining the powder (at 800-1100°C) results in a reduction in surface area and in sintering activity (see Table 6), but it may produce higher green densities (better particle packing in the tape) and higher fired densities. This effect was observed in pressed and sintered pellets (see Table 6).

Table 6. Summary of Sintering Experiments on Y_2O_3-Stabilized ZrO_2 Powder

Sample No.[a]	Green Density, %[b]	Sintering Schedule	Sintered Density, %[b]	Comments
P-216-144-1	36	c	86	As-received powder (44 m^2/g)
P-216-144-2	35	c	85	Powder calcined at 800°C for 1 h (32 m^2/g)
P-216-144-3	36	c	86	Powder calcined at 900°C for 1 h (19 m^2/g)
P-216-145-1	42	c	90	Powder calcined at 1100°C for 1 h (6 m^2/g)
P-216-145-2	42	c	89	Powder calcined at 1100°C for 1 h (6 m^2/g)
T-216-149-1	—	c	—	Tape adhered to Al_2O_3 plate
T-216-150-2	—	c	—	Tape adhered to Al_2O_3 plate
T-234-67	—	c	—	Sintered on ash-less filter paper; sample broke due to filter paper curling
T-234-69-2	40	d	53	No adhesion
T-234-73	33	e	58	No adhesion
T-234-68-2	—	e	—	Tape adhered to Al_2O_3 plate; green tape had absorbed moisture

[a] P- prefix is for pressed pellets; T- prefix is for tapes.

[b] Assuming theoretical density = 5.95 g/cm^3.

[c] Heat to 1500°C in 10 h, hold at 1500°C for 10 h.

[d] Heat to 1300°C in 10 h. hold at 1300°C for 10 h.

[e] Heat to 1300°C in 10 h, hold at 1300°C for 5 h, heat to 1400°C in 1 h, hold at 1400°C for 10 h.

b. Slip Considerations

The objective in slip preparation is to disperse as much powder in as little solvent as possible. Powder dispersal means breaking down agglomerates into individual particles and suspending the individual particles in the liquid medium of the slip. Since the Zircar powder is only lightly agglomerated, high-shear mixing should be adequate for dispersing the powder (ball milling should not be necessary). Thus far, our slips have been prepared by ball milling. Using other techniques to disperse the powder may be advantageous, however, because in ball milling much material is wasted on the walls of the mill and on the grinding media. An ultrasonic probe and a high-shear mixer (Cole Parmer tissue homogenizing system - catalog No. K-4720-00) have been ordered. Either of these devices should be effective in dispersing the powder; one may be more convenient to use than the other.

All of the Y_2O_3-stabilized ZrO_2 slips have been prepared using Cladan (commercially formulated) binder/plasticizer/solvent systems. These systems are quite adequate for producing acceptable tapes. In general, more solvent was required than the amount recommended by Cladan. The higher amounts of solvent were required to facilitate removal of the slip from the ball mill. Less solvent should be adequate when other methods are used to disperse the powder. The Cladan binder system 73150-73151 produced good tapes, but frequently the tape was difficult to handle (sticking to itself after removal from the casting surface). This binder system can be cast on glass. Tapes prepared with this binder system are hygroscopic, which may affect the subsequent sintering behavior of the tape (see Section B.2.d. on sintering considerations). The Cladan binder system 73200 must be cast on Teflon (it adheres to glass). Tapes prepared with this binder system do not adhere to themselves after removal from the casting surface, and they are not hygroscopic. As a result, use of the 73200 binder system appears to be advantageous.

c. Tape Considerations

Casting is relatively straightforward. A pool of slip [$\sim$1 in. x $\sim$5 in. ($\sim$2.54 cm x 12.7 cm)] is poured onto the casting surface, and the doctor blade is moved (by an X-Y recorder at a rate of $\sim$12 in./min) across the surface of the slip. The solvent is then evaporated, preferably in a laboratory hood.

d. Sintering Considerations

The sintering experiments performed to date on tapes and on pressed pellets are summarized in Table 6. Clearly, additional experiments are required to define the conditions necessary for sintering tapes to high density. However, the following conclusions can be drawn from the sintering experiments: (1) heating directly to 1500°C apparently causes adhesion of the tape to the Al_2O_3 plate, (2) heating at 1300°C apparently avoids adhesion (zirconia sinters to itself rather than to the Al_2O_3 plate), but does not produce a high-density product, and (3) tapes that have absorbed moisture (T-234-68-2) adhere to the Al_2O_3 plate when sintered under the same conditions as "dry" tapes (T-234-73).

3. Interconnection and Electrode Fabrication

(R. B. Poeppel,* T. D. Claar,* J. T. Dusek,* J. P. Singh,* R. J. Fousek,* J. J. Picciolo,* and S. Peterson†)

a. Introduction

The objectives of this effort are the evaluation and development of ceramic fabrication processes suitable for fabricating monolithic solid oxide fuel cell configurations which offer the potential of significantly higher power densities than the state-of-the-art tubular SOFC design. The fabrication processes currently under evaluation include tape casting, slip casting, and extrusion.

The fuel cell materials selected for initial investigation include a cobalt/ZrO_2-16 wt % Y_2O_3 cermet for the anode, strontia-doped lanthanum manganite for the cathode, ZrO_2-16 wt % Y_2O_3 for the electrolyte, and magnesia-doped lanthanum chromite as the interconnect material. The gas electrodes are required to be approximately 50% porous, while the electrolyte and interconnect layers must be highly dense ($\geq$93% of theoretical density), with no interconnected porosity or other defects that would allow intermixing of the fuel and oxidant gases.

Experimental efforts during this quarter have focused on materials characterization, further development of tape casting of thin electrode and interconnect layers, electrode fabrication by slip casting and extrusion, sintering studies, and thermal-expansion measurements on candidate cell materials.

b. Materials Characterization

Samples of ZrO_2-16 wt % Y_2O_3 powder prepared by Magnesium Elektron, Inc., Flemington, NJ (Grades SCY16 and SC16Y16), were obtained for evaluation as source materials for anode fabrication. Grade SCY16 is synthesized by calcination of a chemically precipitated intermediate and has a nominal specific surface area range of 0.5-2.0 m^2/g. This grade may be milled to yield Grade SC16Y16, which has a finer particle size distribution and a nominal surface area range of 3-4 m^2/g. Scanning electron microscopy (SEM) of the SCY16 powder revealed agglomerates approximately 10-40 μm in size. These agglomerates consisted of nearly spherical particles approximately 5 μm in diameter. The particles appeared to be highly dense and were well sintered together to form the agglomerates, which were not dispersed by ultrasonic agitation during preparation of the SEM specimens. At high magnification, each of the spherical particles appeared to consist of many submicron-sized ($\sim$0.2 μm) crystallites. The SC16Y16 powder was found to consist of a mixture of submicron-sized particles, resulting from milling of the SCY16 powder, and agglomerates ranging in size from approximately 1 to 10 μm. A few agglomerates of spherical particles larger than 10 μm were also

---

*Materials Science and Technology Division, ANL.

†Undergraduate Research Participant from Rensselaer Polytechnic Institute, Troy, NY.

observed, similar to those found in the unmilled SCY16 material. The milling operation has thus resulted in a rather broad particle size distribution in the SC16Y16 powder.

An order has been placed with Magnesium Elektron, Inc. for 10 lb of Grade SCY16 ZrO_2-16 wt % Y_2O_3 powder. This material will be vibratory milled to reduce the particle size for anode fabrication studies.

Samples of developmental ZrO_2-17 wt % Y_2O_3 powders prepared by Teledyne Wah Chang Albany, Albany, OR, using precipitation processes have also been received for evaluation. Characterization data provided by Teledyne and shown in Table 7 indicate that these materials are of very high surface area.

Table 7. Characterization of ZrO_2-17 wt % Y_2O_3 Powders Supplied by Teledyne Wah Chang Albany

Lot No.	Thermal Treatment	Fisher Subsieve Size, μm	BET Surface Area, m^2/g
A	Calcined at 500°C	4.8	144
B	Calcined at 500°C	4.7	84
C	Dried at 110°C	2.6	201

The sintering behaviors of several yttria-stabilized zirconia powders were compared by cold-pressing 0.5-in. (1.3-cm)-dia pellets at a pressure of 25,500 psi (175.7 MPa) using 5% polyvinyl acetate as binder. The pellets were then sintered at 1400°C in air for 13 h. The results are presented in Table 8. The Zircar product, which is being investigated for use in the electrolyte layer, was the most reactive powder of those studied in this test, achieving a density of 87.7% T.D. Magnesium-Elektron Grade SC16Y16, which is being studied for use in the porous anode, achieved a fired density of 77.1% T.D. The materials supplied by Teledyne Wah Chang had fired densities in the range 60.8-69.2% T.D. It is expected that laundering of the precipitated powders to remove residual chloride and deagglomeration procedures will result in enhanced sintering rates. Further studies on these powders are planned.

One-pound batches of $(La_{0.9}Sr_{0.1})MnO_3$ (cathode material) and $La(Cr_{0.9}Mg_{0.1})O_3$ (interconnect material) powders were also obtained for evaluation. These powders were prepared by A. T. Research, Inc., using the citric acid liquid-mix synthesis route.[10] This process was selected for evaluation based on its proven usefulness in preparing highly reactive, homogeneous powders of complex mixed-oxide compositions. Examinations using SEM revealed that both powders consisted of primary particles approximately 0.2-0.5 μm in size. These particles were only weakly agglomerated as a result of the low calcining temperatures (600-700°C) that are sufficient for crystallizing materials synthesized by this process. Both the

Table 8. Results of Sintering Various ZrO_2-Y_2O_3 Powders at 1400°C for 13 h in Air

Material	Green Density, g/cm^3[a]	Fired Density		Firing Weight Loss, %
		g/cm^3	% T.D.[b]	
A[c]	2.35	4.12	69.2	15.0
B[c]	2.37	3.62	60.8	9.4
C[c]	1.65	3.88	65.2	25.3
Zircar[d]	2.49	5.22	87.7	7.5
SCY16[e]	3.04	3.37	56.6	5.3
SC16Y16[e]	3.29	4.59	77.1	4.8

[a]Corrected for binder and volatile contents.

[b]Theoretical density ∿5.95 g/cm^3.

[c]Teledyne Wah Chang Albany, Albany, OR.

[d]Zircar Products, Inc., Florida, NY.

[e]Magnesium Elektron, Flemington, NJ.

$La(Cr_{0.9}Mg_{0.1})O_3$ (AT-1) and $(La_{0.9}Sr_{0.1})MnO_3$ (AT-2) powders have a finer particle size distribution and are more uniform than the corresponding compositions prepared by Cerac via high-temperature synthesis.

BET surface area measurements performed on these lanthanum-based perovskite powders indicated higher surface areas for those materials prepared by the liquid-mix process than for those prepared by calcining, as shown in Table 9.

Table 9. Summary of BET Surface Area Measurements

Material	Surface Area, m^2/g	
	Calcining Process[a]	Liquid Mix Process[b]
$La(Cr_{0.9}Mg_{0.1})O_3$	0.66	4.1
$(La_{0.9}Sr_{0.1})MnO_3$	0.64	7.1

[a]Cerac, Milwaukee, WI.

[b]A. T. Research Company, Vichy, MO.

In our earlier studies on fabrication of Co/ZrO_2-Y_2O_3 anodes, J. T. Baker reagent grade cobalt oxide (-325 mesh) was used as a starting material. During this quarter, three different chemical grades of cobalt oxide powder were obtained from Hall Chemical Company, Cleveland, OH, for

evaluation. These materials are designated as grades 70-71% cobalt (-325 mesh), 72-73% cobalt (-325 mesh), and 71.5% cobalt and are typically used in the manufacture of catalysts. The 70-71%-cobalt and 72-73%-cobalt materials appear by SEM to consist of soft agglomerates approximately 2-40 μm in size; these agglomerates are composed of submicron particles and seem to be of relatively high surface area. The 71.5%-cobalt material had not been screened and thus consisted of coarser agglomerates than the other two grades.

In addition, samples of technical-grade nickel oxide powder have been received from Hall Chemical and the International Nickel Corporation (INCO) for evaluation in the fabrication of Ni/ZrO_2-Y_2O_3 anodes. These powders are currently being analyzed with scanning electron microscopy.

c. Tape-Casting Studies

Tape-casting experiments were conducted during this quarter on the fabrication of anode, cathode, and interconnect materials. Tapes were fabricated using the same general procedures as described in the last quarterly report.[11] The results of powder settling experiments have indicated that Menhaden Z-3 fish oil is a very effective deflocculating and dispersing agent for the powders of interest, and fish oil additions are now being made to the commercial tape-casting binders used in these studies. A general summary of the tape-casting experiments performed in this program is presented in Tables 10-13.

Disks approximately 1 in. (2.54 cm) in diameter were punched from selected anode and cathode tapes for burnout and sintering studies. Organic burnout consisted of heating in air from room temperature to 400°C over a period of 8 h and holding at 400°C for 1 h. The specimens were then heated to the desired sintering temperature at a rate of 50 to 100°C/h.

Tapes ZYC-1, -2, -3, and -4 (Table 10) from our previous studies of the Co/ZrO_2-Y_2O_3 anode material contained 30 vol % cobalt metal phase after reduction of the cobalt oxide starting material. These studies have been extended to include a composition corresponding to 50 vol % cobalt, with tape-casting slips ZYC-5 and -6. Slip ZYC-5 was prepared with Magnesium Elektron Grade SCY16 ZrO_2-Y_2O_3 powder (0.29 m^2/g surface area) while slip ZYC-6 was formulated with Magnesium Elektron Grade SC16Y16 ZrO_2-Y_2O_3 powder having a finer particle size distribution (3.8 m^2/g surface area).

Disk specimens were punched from tapes ZYC-5 and -6, as well as from previously fabricated ZrO_2-Y_2O_3/cobalt oxide tapes ZYC-2, -3, and -4 for evaluation of their sintering behavior. Specimens of tapes prepared from the finer particle size Grade SC16Y16 ZrO_2-Y_2O_3 powder underwent significantly greater diametral shrinkages (18.3%) during sintering at 1300°C for 30 min than did those fabricated from the Grade SCY16 material (~1%). The sintered specimens from the SC16Y16 material had fired geometric densities of 4.5-4.7 g/cm^3 and could be readily handled. These density values correspond to a porosity level of approximately 26% before the reduction step. The poorly sintered specimens from the SCY16 zirconia powder had fired densities of 2.3-2.5 g/cm^3, essentially the same as the green tape density. These disks were very fragile and difficult to handle without fracturing. Differences in cobalt oxide content (30 vs 50 vol % metallic cobalt equivalent) had no significant effect on sintering behavior.

Table 10. Summary of Cobalt/ZrO_2-Y_2O_3 Anode Tape-Casting Experiments

Slip No.	Composition	Casting Thickness	Comments
ZYC-1	25 g ZrO_2-Y_2O_3 (SC16Y16) 34.4 g cobalt oxide (Baker, -325) 51 g Cerbind B-62	A-10 mils[a]	Air bubbles present in tape.
ZYC-2	26.4 g ZrO_2-Y_2O_3 (SC16Y16) 23.6 g cobalt oxide (Baker, -325) 40 mL methylene chloride 50 g Cerbind 73115	A,C-10 mils B-20 mils	Solvent evaporated before binder addition.
ZYC-3	26.4 g ZrO_2-Y_2O_3 (SCY16) 23.6 g cobalt oxide (Baker, -325) 40 mL methylene chloride 33.6 g Cerbind 73115	A,B-20 mils	Fish oil deflocculant. Solvent evaporated before binder addition.
ZYC-4	26.4 g ZrO_2-Y_2O_3 (SCY16) 23.6 g cobalt oxide (Baker, -325) 27 g Cerbind 73151 34.2 g Cerbind 73150	A,B,C-20 mils	Fish oil deflocculant.
ZYC-5	16.1 g ZrO_2-Y_2O_3 (SCY16) 33.9 g cobalt oxide (Baker, -325) 20.2 g Cerbind 73151 33.9 g Cerbind 73150 0.5 g Z-3 fish oil	A,B-20 mils	Tapes easily removed from substrate; no sticking. Tapes very strong, quite stretchable before tearing.
ZYC-6	16.1 g ZrO_2-Y_2O_3 (SC16Y16) 33.9 cobalt oxide (Baker, -325) 20.2 g Cerbind 73151 33.9 g Cerbind 73150 0.5 g Z-3 fish oil	A,B-20 mils	Similar to XYC-5 above.
ZYC-7	16.1 g ZrO_2-Y_2O_3 (Zircar) 33.9 g cobalt oxide (Baker, -325) 41.85 g Cerbind 73151 35.6 g Cerbind 73150 0.8 g Z-3 fish oil	A,B-20 mils	Small agglomerates present. Tapes very tacky; some stretching occurred when removing. Tapes stuck to themselves. No further testing done.
ZYC-8	16 g ZrO_2-Y_2O_3 (SC16Y16) 34 g cobalt oxide (Hall 70-71%) 53 g Cerbind 73151 33.3 g Cerbind 73150 0.5 g Z-3 fish oil	A,B-20 mils	Tapes removed relatively easily. Somewhat tacky.
ZYC-9	16.15 g ZrO_2-Y_2O_3 (SC16Y16) 34.15 g cobalt oxide (Hall, 71.5% unscreened) 47 g Cerbind 73151 35.8 g Cerbind 73150 0.5 g Z-3 fish oil	A,B-20 mils	Extremely tacky; tapes stuck to themselves upon removal. Relatively easy removal from substrate.
ZYC-10	16 g ZrO_2-Y_2O_3 (SC16Y16) 34 g cobalt oxide (Hall 70-71%) 42.3 g isopropyl alcohol 61.1 g 73200 binder conc. 0.5 g Z-3 fish oil	A,B,C,D-20 mils	A - viscosity - 800 cp - surface tearing due to low viscosity. B,C - viscosity - 1264 cp D - viscosity - 4000 cp Tapes removed relatively easily.

[a] 1 mil = 0.001 in. = 0.0254 mm.

Table 11. Summary of Nickel/ZrO_2-Y_2O_3 Anode Tape-Casting Experiments

Slip No.	Composition	Casting Thickness	Comments
ZYN-1	16.9 g ZrO_2-Y_2O_3 (SC16Y16) 33.1 g nickel oxide (INCO) 30 g isopropyl alcohol 57.5 g 73200 binder conc. 0.5 g Z-3 fish oil	A,B,C,D-20 mils[a]	B,C,D - considerable shrinkage. D - some agglomerates. Tapes easily removed from substrate. Evaporated 4.3 g of solvent to get a viscosity of 1468 cp.
ZYN-2	16.9 g ZrO_2-Y_2O_3 (SC16Y16) 33.1 g nickel oxide (Hall 76%, -325) 30 g isopropyl alcohol 57.7 g 73200 binder conc. 0.5 g Z-3 fish oil	A,B,C,D-20 mils	Some shrinkage on all tapes. D - some agglomerates. Tapes easily removed from substrate. Evaporated 6.2 g of solvent to get a viscosity of 1968 cp.
ZYN-3	16.9 g ZrO_2-Y_2O_3 (SC16Y16) 33.1 g nickel oxide (Hall 76%, -325) 20.5 g Cerbind 73151 35.1 g Cerbind 73150 0.5 g Z-3 fish oil	A,B-20 mils	Tapes easily removed from substrate. Many agglomerates present.
ZYN-4	16.9 g ZrO_2-Y_2O_3 (SC16Y16) 33.1 g nickel oxide (INCO) 30.3 g Cerbind 73151 36.3 g Cerbind 73150 0.5 g Z-3 fish oil	A,B-20 mils	Tapes easily removed from substrate, somewhat tacky and stretchy.
ZYN-5	16.9 ZrO_2-Y_2O_3 (SC16Y16) 33.1 g nickel oxide (Hall 76%, -325) 20.6 g Cerbind 73151 36.6 g Cerbind 73150 0.5 g Z-3 fish oil	A-20 mils	Tapes easily removed from substrate. Large agglomerates present. Same composition as ZYN-3.

[a] 1 mil = 0.001 in. = 0.0254 mm.

The sintered specimens from tapes ZYC-2 and -6 fabricated from SC16Y16 zirconia were subsequently reduced in hydrogen at 1100°C for 2 h to form the Co/ZrO_2-Y_2O_3 cermet required for the anode. The reduced disks had densities of 4.3-4.4 g/cm^3, corresponding to porosities of approximately 40%. The final disks were 0.003 to 0.005 in. (0.076-0.127 mm) thick and remained flat during the sintering and reduction processes. They had ample strength and ductility to permit handling without incurring any damage. The microstructures of the sintered and reduced Co/ZrO_2-Y_2O_3 anode tapes as revealed by optical microscopy are shown in Figs. 21 and 22 for 30- and 50-vol % cobalt contents, respectively. The cobalt particles range in size from about 1 to 15 μm. Many of the cobalt particles have linked up to form an elongated interconnected morphology, especially in the 50-vol % cobalt material.

Table 12. Summary of $(La,Sr)MnO_3$ Cathode Tape-Casting Experiments[a]

Slip No.	Composition	Casting Thickness	Comments
LM-1	51 g $(La,Sr)MnO_3$ (Cerac) 51 g Cerbind B-62	A-10 mils[b]	Significant wrinkling of tape. Some air bubbles present in tape.
LM-2	50 g $(La,Sr)MnO_3$ (Cerac) 30 mL methylene chloride 25 g Cerbind 73115	A-20 mils	Fish oil deflocculant. Solvent evaporated before binder added.
LM-3	50 g $(La,Sr)MnO_3$ (A.T. Res.) 40 mL methyl chloroform 50 g Cerbind 73115	A,B,C-20 mils	Fish oil deflocculant. Solvent evaporated before binder added.
LM-4	25 g $(La,Sr)MnO_3$ (A.T. Res.) 55.3 g Cerbind 73115 3 mL methyl chloroform	A,B-20 mils	Fish oil deflocculant
LM-5	45 g $(La,Sr)MnO_3$ (A.T. Res.) 32 g Cerbind 73151 30.3 g Cerbind 73150 8 mL methyl chloroform	A,B,C,D-20 mils	Fish oil deflocculant
LM-6	60 g $(La,Sr)MnO_3$ (Cerac) 29.25 g Cerbind 73151 36.1 g Cerbind 73150 0.5 g Z-3 fish oil	A,B,C-20 mils	Tapes easily removed from substrate.
LM-7	20 g $(La,Sr)MnO_3$ (A.T. Res.) 55.2 g Cerbind 73115 (old mixture) 0.5 g Z-3 fish oil 6 g chloroform	A,B-20 mils	Tapes easily removed from substrate. Binder "patches" visible on underside of tapes.
LM-8	20 g $(La,Sr)MnO_3$ (A.T. Res.) 55 g Cerbind 73115 0.5 g Z-3 fish oil	A,B-20 mils	Tapes easily removed from substrate. Binder "patches" visible on underside of tape.

[a] $(La_{0.9}Sr_{0.1})MnO_3$.

[b] 1 mil = 0.001 in. = 0.0254 mm.

Additional sintering studies are being conducted on anode tapes fabricated from Grade SC16Y16 ZrO_2-Y_2O_3 powder to establish the sintering time/temperature schedule required to produce 50% porosity. Specimens of tape ZYC-6 sintered at 1200°C for 30 min had densities of 3.2-3.3 g/cm^3, while those sintered at 1300°C for 10 min had densities of 4.1-4.5 g/cm^3. If no further densification occurs during the hydrogen reduction step, specimens having an air-fired density of 4.3 g/cm^3 will have a porosity of approximately 50% after reduction of the cobalt oxide phase to metallic cobalt.

Three different chemical grades of cobalt oxide powder have been received from Hall Chemical Company for comparison with the reagent grade material used in the present studies. Tapes ZYC-8, ZYC-9, and ZYC-10 have been cast from slips formulated from mixtures of these powders with Grade SC16Y16 ZrO_2-Y_2O_3, and sintering studies are in progress.

Table 13. Summary of $La(Cr,Mg)O_3$ Interconnect Tape-Casting Experiments[a]

Slip No.	Composition	Casting Thickness	Comments
LC-1	50 g $La(Cr,Mg)O_3$ (Cerac) 50.1 g Cerbind 73115	A-10 mils[b] B-20 mils C,D-5 mils	Tapes easily removed from glass.
LC-2	51.5 lanthanum chromite (Cerac) 51.5 g Cerbind B-62	A-10 mils	Air bubbles present in tape.
LC-3	62.1 g $La(Cr,Mg)O_3$ (Cerac) 51.8 g Cerbind 73115	A,B-10 mils C-5 mils	No deflocculant added.
LC-4	109.5 g $La(Cr,Mg)O_3$ (Cerac) 10 cc methyl chloroform 48.4 g Cerbind 73115	A,B,C-10 mils	Corn oil deflocculant. Excess solvent removed by evacuation before casting.
LC-5	45 g $La(Cr,Mg)O_3$ (A.T. Res.) 26 g Cerbind 73151 31.1 g Cerbind 73150	A,B,C-10 mils	Fish oil deflocculant
LC-6	65 g $La(Cr,Mg)O_3$ (A.T. Res.) 30.3 g isopropyl alcohol 60.3 g 72300 (binder conc.) 0.5 g Z-3 fish oil	A,C-10 mils	Last 5 g powder added after binder. Agglomerates - probably due to late addition of powder. A - some tearing of the skin.

[a] $La(Cr_{0.9}Mg_{0.1})O_3$.

[b] 1 mil = 0.001 in. = 0.0254 mm.

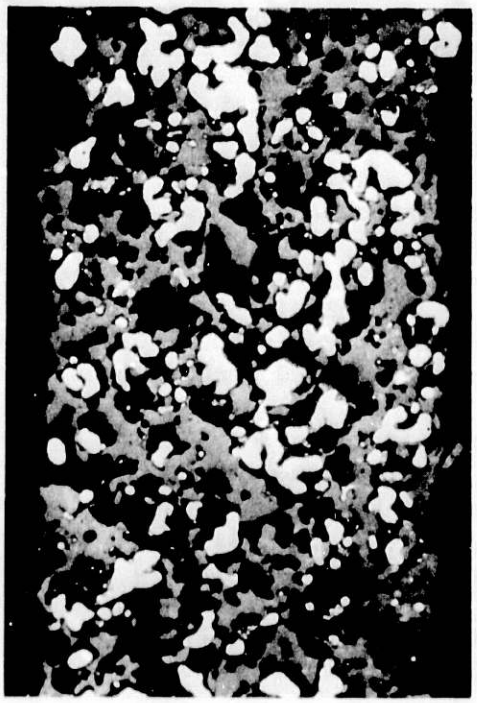

Fig. 21.

Optical Micrograph of Co/ZrO_2-Y_2O_3 Anode Tape Containing ~30 vol % Cobalt. Sintered 30 min at 1300°C in air and reduced 2 h at 1100°C in H_2. (Tape ZYC-2-B-4)

Fig. 22.

Optical Micrograph of Co/ZrO_2-Y_2O_3 Anode Tape Containing ∿50 vol % Cobalt. Sintered 30 min at 1300°C in air and reduced 2 h at 1100°C in H_2. (Tape ZYC-6-A-1)

Nickel is also being considered as a candidate anode material, because of its greater resistance to electrochemical oxidation and lower cost relative to cobalt. Tapes have been fabricated using commercial nickel oxide powders produced by Hall Chemical Company and INCO (see Table 11). Specimens are currently being sintered and characterized microstructurally.

Sintering studies were performed on specimens of $(La_{0.9}Sr_{0.1})MnO_3$ cathode tapes (see Table 12) to investigate the effects of sintering schedule and starting material characteristics on densification and microstructure. Specimens from tape LM-2, prepared from the powder synthesized by Cerac, were sintered for 30 min at 1200 and 1300°C to densities of 4.0 g/cm^3 (∿39% porosity) and 5.1 g/cm^3 (∿22% porosity), respectively. This tape had a green density of ∿2.3 g/cm^3. Tapes prepared from the more reactive powder synthesized by A. T. Research exhibited much greater densification under the same conditions. Tapes LM-3 and -5, which had green densities of 1.9-2.1 g/cm^3, sintered to densities of 5.7-5.9 g/cm^3 (10-14% porosity) and 6.1-6.5 g/cm^3 (2-8% porosity) at 1200 and 1300°C, respectively. Tape LM-4 had a lower green density of 1.6 g/cm^3 and sintered to densities of 4.8 g/cm^3 (27% porosity) and 5.8 g/cm^3 (12% porosity) at these same temperatures. The sintered specimens ranged in thickness from 3 to 8 mils. The scanning electron micrographs shown in Figs. 23 and 24 compare the microstructures developed by sintering at 1200°C for tapes made from the $(La_{0.9}Sr_{0.1})MnO_3$ synthesized by high-temperature reaction (Cerac) and by the liquid-mix technique (A. T. Research).

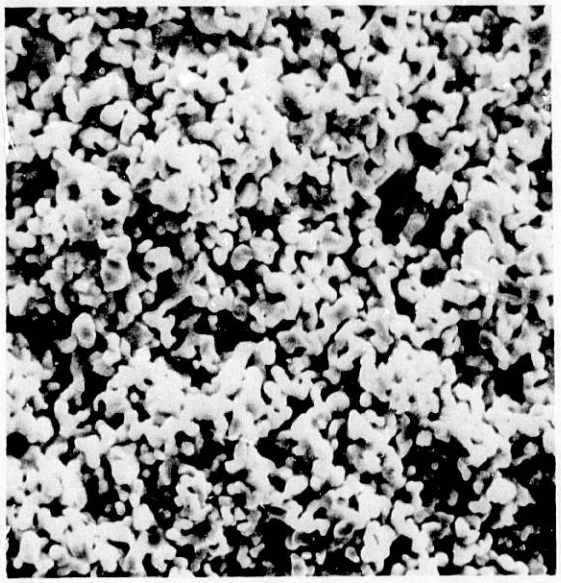

Fig. 23. Scanning Electron Micrograph of Tape from Cerac $(La_{0.9}Sr_{0.1})MnO_3$ Sintered 30 min at 1200°C. (Tape LM-2-6)

Fig. 24. Scanning Electron Micrograph of Tape from A. T. Research $(La_{0.9}Sr_{0.1})MnO_3$ Sintered 30 min at 1200°C. (Tape LM-3-B-4)

More recent sintering results from tape LM-6 (Cerac powder) indicate that densities of 3.4 g/cm^3 (~48% porosity) have been altered by sintering 30 min at 1200°C. Microstructural analyses of these specimens will be performed during the next reporting period.

Progress is also being made on the sintering of the $La(Cr_{0.9}Mg_{0.1})O_3$ electrode interconnect material. This material must be of high density (≥93%) with no continuous porosity, in order to avoid intermixing of fuel and oxidant gases. Specimens of tape LC-5 (see Table 13) prepared from the fine-particle-size magnesia-doped lanthanum chromite powder synthesized by A. T. Research were heated to 400°C in air to burn out the organics and then transferred to a controlled-atmosphere furnace for sintering at a low-oxygen partial pressure [10^{-9} to 10^{-12} atm ($0.1\text{-}1.1 \times 10^{-4}$ mPa)]. The sintering was conducted at 1550°C for 1 h in a reducing atmosphere of approximate composition 200 CO/1 CO_2. The sintered tapes were ~1.8 mils thick. Although it was difficult to accurately determine geometric densities of the sintered interconnect specimens because of warpage, it is estimated that densities of ~90% T.D. were achieved. This is a significant improvement over the sintering behavior observed for the coarser Cerac $La(Cr_{0.9}Mg_{0.1})O_3$ powder sintered previously in air at 1500°C, in which essentially no densification occurred. Figure 25 is an SEM micrograph of an interconnect specimen sintered recently under more reducing conditions. Additional work is planned in an effort to further increase the fired density, to eliminate the warpage, and to minimize the grain growth occurring during the densification step.

Fig. 25.

Scanning Electron Micrograph of Tape from A-T Research $La(Cr_{0.9}Mg_{0.1})O_3$ Sintered 1 h at 1550°C in 200 CO/1 CO_2. (Tape LC-5-A-2)

Plans are being made to evaluate alternative means of dispersing the powders into the tape-casting slips, in order to minimize the presence of agglomerates and to obtain higher green densities and more uniform particle distributions. Equipment is being obtained for investigating the use of vibratory milling, ultrasonic dispersion, and high-shear mixing for achievement of these goals.

d. Slip-Casting Studies

Anode and cathode materials have also been fabricated via slip casting into planar configurations with internal cylindrical gas flow channels. Water-based slips of ZrO_2-10 wt % Y_2O_3/cobalt oxide; and of $(La_{0.9}Sr_{0.1})MnO_3$ were prepared by ball milling overnight, using ammonium alginate as a binder. The slips were then cast into plaster molds with metal core pins to form the gas flow channels. After removal from the mold, the cast shapes were dried and sintered for characterization.

Slip S4 consisted of a mixture of 52.7 g ZrO_2-10 wt % Y_2O_3 (Cerac), 47.3 g cobalt oxide (Baker), 0.65 g ammonium alginate, and 35 g H_2O. After this mixture was ball-milled overnight, several castings were made by gravity feeding into a small plaster mold with a cavity approximately 1-1/16 in. long x 11/16 in. wide x 1/8 in. high (27.0 x 17.5 x 3.2 mm) and containing 7-core pins 0.06 in. (1.52 mm) in diameter. The dried castings were fired in air to a temperature of 825°C for binder burnout. Specimens were then fired either in air or vacuum at 1450°C for 15 min to produce partially sintered structures. These sintered bodies were subsequently further sintered in hydrogen for 2 h at 1100°C to reduce the cobalt oxide to metallic cobalt, as required for fuel cell anode operation. A low-magnification photograph of a cross section from the air-sintered and hydrogen-reduced specimen is shown in Fig. 26. Several cracks were observed in the web areas between gas channels, possibly due to nonuniform filling of the mold with

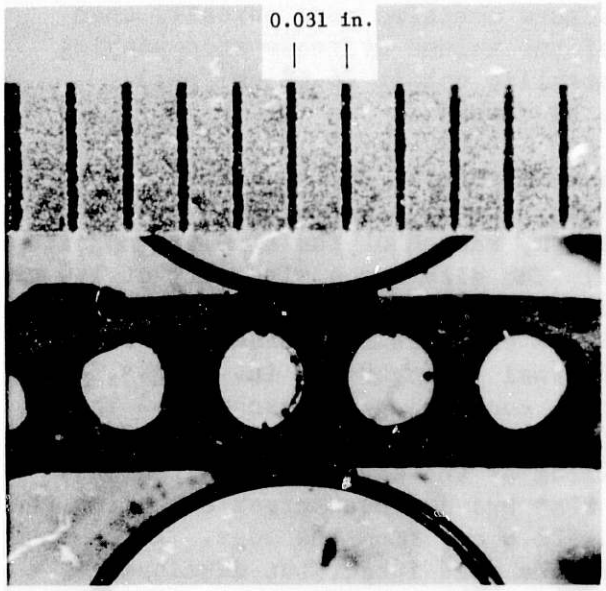

Fig. 26.

Cross Section through Slip-Cast ZrO_2-Y_2O_3/Cobalt Oxide after Sintering in Air (15 min at 1450°C) and Reduction in Hydrogen (2 h at 1100°C)

slip during casting. The gas channels were ∿0.05 in. (1.30 mm) in diameter, the webs between channels were ∿0.025 in. (0.64 mm) wide, and the total thickness was ∿0.09 in. (2.30 mm).

Figures 27a and 27b are optical micrographs of the anode specimens cast from slip S4, after air sintering and hydrogen reduction, respectively. The air-sintered structure contains some porosity about 3-25 μm in size, most of which does not appear to be interconnected. The hydrogen-reduced structure contains discrete particles of metallic cobalt ranging in size from ∿2 to 25 μm, fairly uniformly distributed in the

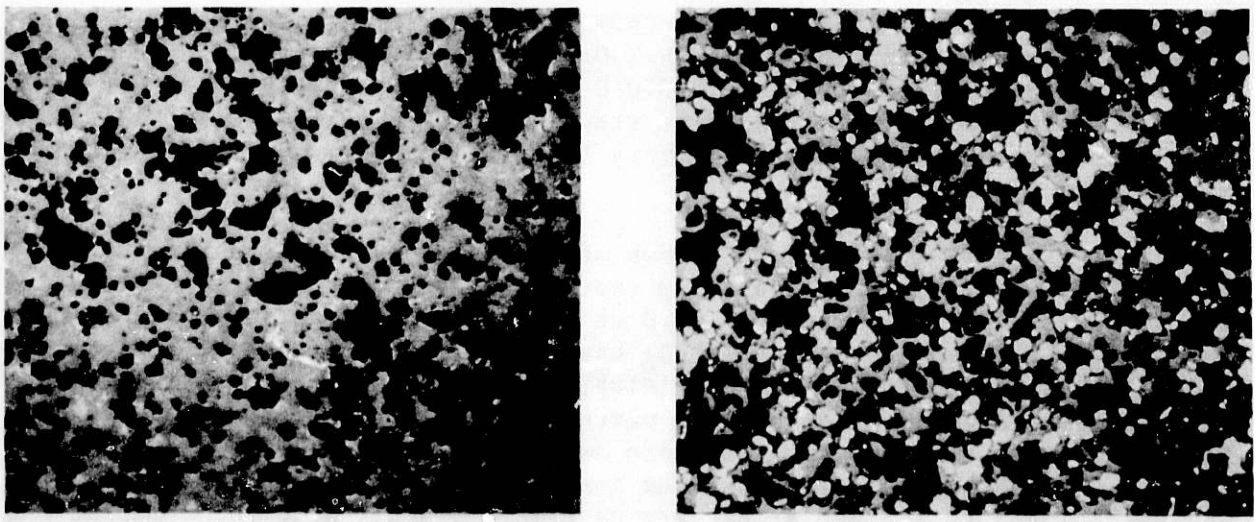

Fig. 27. Optical Micrographs of Slip-Cast ZrO_2-Y_2O_3/Cobalt Oxide. (a) Sintered in air at 1450°C for 15 min; (b) reduced in hydrogen at 1100°C for 2 h.

ZrO_2-Y_2O_3 matrix. The reduced microstructure contains more porosity than the air-sintered structure as a result of the volume decrease accompanying the reduction of CoO (11.6 cm^3/mol) to metallic cobalt (6.62 cm^3/mol). However, much of the porosity appears to be closed.

Slip S4-A was prepared as a mixture of 105.4 g ZrO_2-10 wt % Y_2O_3, 94.6 g cobalt oxide, and 1.3 g ammonium alginate in 80 mL H_2O. After the slip was ball-milled for about 4 h, the pH of the slip was adjusted to 6-7 by addition of ammonium hydroxide. The slip had a viscosity of 140 cP (Brookfield spindle No. 5 @ 100 rpm) and a specific gravity of 2.48 g/cm^3 after further ball milling overnight. Three castings were made from this slip in a larger plaster mold with an internal cavity 3-7/8 in. long × 3 in. wide × 1/8 in. (98.4 × 76.2 × 3.18 mm) high containing 32 core pins. The slip was forced into the mold under an argon pressure of 12-15 psig (82.7-103.4 kPa) in order to obtain better filling of the cavity in web regions. The first casting made at 12 psig (82.7 kPa) had a linear crack extending the full length of the piece about 1-1/8 in. (28.6 mm) from the edge. The second casting at this pressure was removed from the mold intact but developed a small crack about 1 in. (2.54 cm) from an edge shortly after removal. The cause of these cracks was not obvious. It is possible that a core pin was slightly bowed in the region of the cracks, resulting in a thinner and weaker wall, or the pieces may have been slightly damaged during removal of the core pins. The third casting, made at a pressure of 15 psig (103.4 kPa), split into two pieces upon removal from the mold, as a result of the casting sticking to both lateral surfaces of the mold. The casting was well developed in the web regions except for three small segments about 1 in. (2.54 cm) long that were not completely filled.

Specimens from a casting made at 12 psig (82.7 kPa) were dried and then sintered under two conditions. Firing in hydrogen directly at 1400°C for 15 min resulted in the development of numerous large and small cracks. These cracks were very likely a result of the reduction of cobalt oxide to metallic cobalt and the accompanying release of water vapor during heatup, before sintering of the ZrO_2-Y_2O_3 occurred. More promising results were obtained by firing in air at 1300°C for 15 min to partially sinter the structure, followed by the reduction step in hydrogen at 1100°C for 2 h. This procedure resulted in a crack-free body, which is currently undergoing microscopic examination.

Cobalt/ZrO_2-Y_2O_3 anodes of compositions corresponding to 50 vol % Co were also formed by slip casting, sintered, and characterized microstructurally. A mixture of 67.8 wt % Baker reagent grade cobalt oxide and 32.2 wt % Cerac ZrO_2-10 wt % Y_2O_3 was ball-milled in methanol, dried, and calcined at 1200°C. After calcining, the powder was again ball-milled in methanol and dried. This powder mixture was then dispersed in water to form slip S-5, using ammonium alginate as a binder and NH_4OH as a deflocculant. Slip S-5A was formulated the same as S-5, but without the milling and calcining steps. Both slips were cast in a plaster mold to form flat anode structures containing cylindrical gas flow passages. After drying, the castings were sintered at 1450°C for 30 min in air, then fired 2 h at 1100°C in H_2 to reduce the cobalt oxide to metallic cobalt. Scanning electron micrographs of the resulting microstructures are compared in Fig. 28. The calcining/milling procedures employed with casting S-5 resulted in

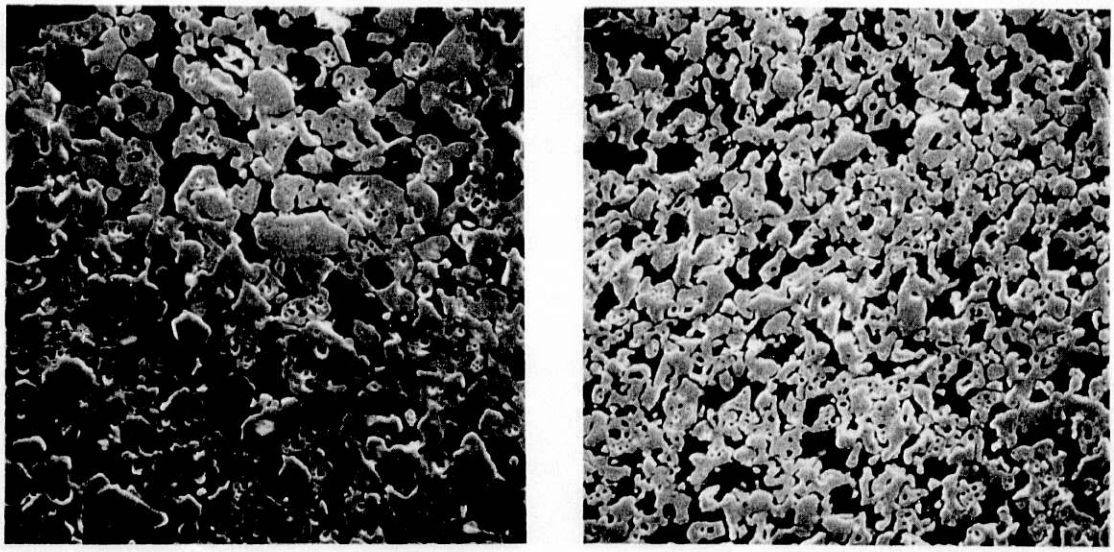

(a) (b)

Fig. 28. Scanning Electron Micrographs of Polished Cross Sections from Slip-Cast Co/ZrO_2-Y_2O_3 Anodes (a) S-5A and (b) S-5

smaller particle sizes for both the cobalt and ZrO_2-Y_2O_3 phases and a somewhat more finely dispersed microstructure. The cobalt particles in both specimens have retained some internal porosity as a result of the volume decrease associated with reduction of the cobalt oxide particles to cobalt. The X-ray image maps for Zr and Co indicated reasonably uniform dispersions of cobalt in the ZrO_2-Y_2O_3 matrix.

Slip casting of cathode structures was also investigated, using the strontia-doped lanthanum manganite powder prepared by A. T. Research. Initial casting results using gravity feeding of the slip into the plaster mold indicated only partial filling of the cavity. Further development work will be required to adjust the rheology of these slips for better control of their flow characteristics and casting rates.

e. Extrusion Studies

The efforts on fabrication of flat electrode structures with gas flow channels are currently being redirected toward extrusion processes, which have greater potential for commercial mass production than slip casting. An existing die has been modified to enable extrusion of hollow cylindrical shapes having wall thicknesses of ∿15 mils and inside diameters of ∿60 mils. This geometry simulates a single gas channel within an electrode structure and will permit determination of suitable ceramic mix formulations and extrusion parameters.

Extrusion mixes of calcia-stabilized zirconia (Zircoa B) and cobalt oxide/calcia-stabilized zirconia were prepared by mixing the powders with water. Ammonium alginate, methocellulose, and Mobilcer "C" (Mobil Oil Corp.) were used as organic additives to provide the rheological properties required for extrusion. Hollow tubes were extruded successfully with both materials. After they were dried under ambient conditions, specimens were

sintered in air at temperatures of 1200, 1300, and 1400°C. Figures 29a and 29b are SEM micrographs of a fractured surface from a cobalt oxide/ZrO_2-5 wt % CaO tube sintered in air at 1300°C. The wall thickness of the sintered tube varied between approximately 12 and 14 mils. Hydrogen reduction of the sintered tubes, as well as microstructural characterizations, will be performed. In parallel, design of a multi-channel extrusion die is continuing, based on a review of the literature and discussions with extrusion experts in outside organizations.

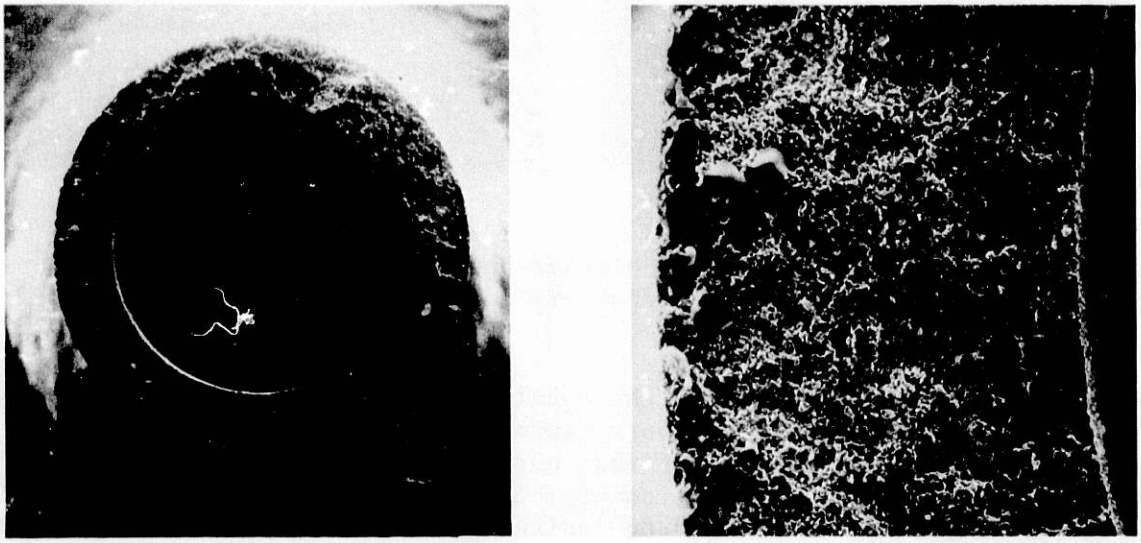

(a) (b)

Fig. 29. Scanning Electron Micrographs of Extruded Cobalt Oxide/SrO_2-CaO Tube Sintered at 1300°C in Air: (a) Cross Section of Tube; (b) Higher Magnification of Wall.

f. Thermal Expansion Measurements

The thermal expansion behavior of the $La(Cr_{0.9}Mg_{0.1})O_3$ interconnect material has been measured and reported previously.[11] During this quarter, rectangular specimens of the ZrO_2-16 wt % Y_2O_3 electrolyte and $(La_{0.9}Sr_{0.1})MnO_3$ cathode material were fabricated by cold-pressing and sintering, and their thermal expansions were determined in a Theta Dilatronic II dilatometer. The resulting thermal expansion curves are shown in Fig. 30. The ZrO_2-16 wt % Y_2O_3 specimen exhibited a mean thermal expansion coefficient of 10.3 x 10^{-6}/°C between 25 and 1000°C, while the $(La_{0.9}Sr_{0.1})MnO_3$ specimen had a corresponding value of 10.6 x 10^{-6}/°C. These values compare with the mean coefficient of thermal expansion of 9.6 x 10^{-6}/°C determined previously for the interconnect material. Anode specimens of ZrO_2-Y_2O_3/50 vol % Co have also been fabricated and will be tested as soon as the dilatometer system has been modified to permit use of H_2/H_2O or CO/CO_2 gas mixtures.

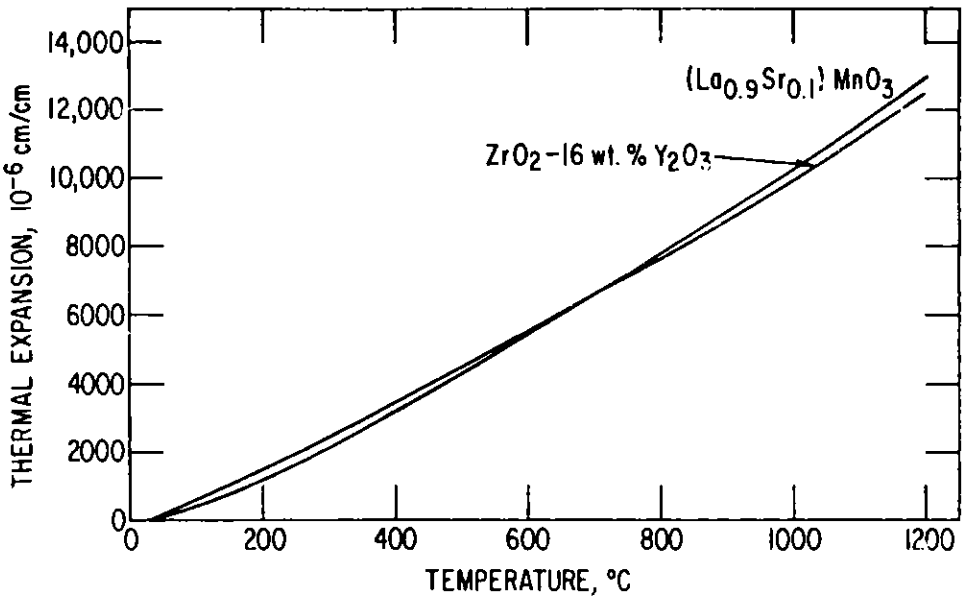

Fig. 30. Thermal Expansion Curves Measured for ZrO_2-16 wt % Y_2O_3 and $(La_{0.9}Sr_{0.1})MnO_3$

4. Electrical Conductivity Measurements in Ceramics
(V. L. Richards* and R. B. Poeppel†)

The information which can be obtained from electrical conductivity measurements of oxide ceramics can be classified as follows:

1. Total conductivity as a function of environmental temperature, oxygen chemical potential, and dropout level.

2. Dominant carrier species and contribution of minority carrier species.

3. Microstructural effects.

4. Electrode behavior.

The measurement of total conductivity as a function of oxygen partial pressure, temperature, and dropout level is useful in two ways: (1) Data may be obtained from prototype materials under simulated operating conditions, and (2) The effects of varying processing conditions, composition, and operating conditions may be related to the data through defect equilibria and analysis of microstructure.

*Assistant Professor at the Illinois Institute of Technology, Chicago, IL.
†Materials Science and Technology Division, ANL.

Various approaches can be used to characterize the contributions of ionic carrier species, as opposed to electronic carrier species to the total conductivity. The effects of microstructural features such as grain boundaries and distributed second phases have been measured in solid oxide electrolytes by observing the relaxation of frequency-dependent sample impedances as originally done by Bauerle.[12] Microstructural effects have been observed in electronic conductors through the analysis of bias effects or conductivity of polycrystalline materials and materials with a distributed second phase coating the grain boundary.[13] An analysis of the electrolyte/electronic/conductor/gas-phase microsystem shows that significant rate effects (polarization) of oxygen cells can occur even in low current loadings such as in an oxygen gauge.[14] The following discussion first presents the parameters of the test design, then how these parameters are combined to meet the objectives of total conductivity measurement, carrier species determination, examination of microstructural effects, and electrode behavior.

a. Parameters of Test Design

The test signal used can be characterized by level and frequency. The test signal may be approaching zero as in the open-circuit EMF measurements or at some level low enough to avoid polarization. On the other hand, nonohmic behavior at varying dc signal levels has been interpreted as a grain boundary effect.[13] Alternating-current signals may be used to obviate electrode polarization and may be varied in frequency to study second-phase and electrode effects in ionic conductors.[12]

The arrangement and chemical nature of the electrodes are other variables which can be applied according to the conductivity range of the material and the test objective. The four-probe method commonly takes two forms: (1) bar specimen and (2) van der Pauw specimen. The bar specimen has current electrodes arranged on the extremes with voltage probes arranged between the current electrodes on a gauge length of known cross section and length.[15] Another approach is the van der Pauw method[16] which can, in theory, be applied to an arbitrarily shaped specimen, resulting in a conductivity expression of the form

$$1 = e^{-\left(\pi V_A t/I_A \rho\right)} + e^{-\left(\pi V_B t/I_B \rho\right)} \qquad (1)$$

where I and V are current and voltage between contact points, t is sample thickness and ρ is the resistivity of the material. In the three-probe technique, the third probe takes the form of a guard ring[17] or a point electrode,[14] depending upon the objective of the experiment. If the third probe is a guard ring or volume guard, it is driven by a unity gain amplifier to the same voltage as the nearby electrode. This prevents surface or gas-phase currents from contributing to the current in the measuring circuit, as indicated in Fig. 31. Another three-probe arrangement which has been used for examining the difference in oxygen chemical potential in the gas phase vs the solid electrolyte surface is the point electrode arrangement shown in Fig. 31d.[14] Also shown is the two-pole arrangement (Fig. 31e) which is useful when the conductivity of the sample is low enough that electrode effects can be neglected. The dimensional relationships for maximizing the surface path length are shown. Chemical reversibility is another consideration of

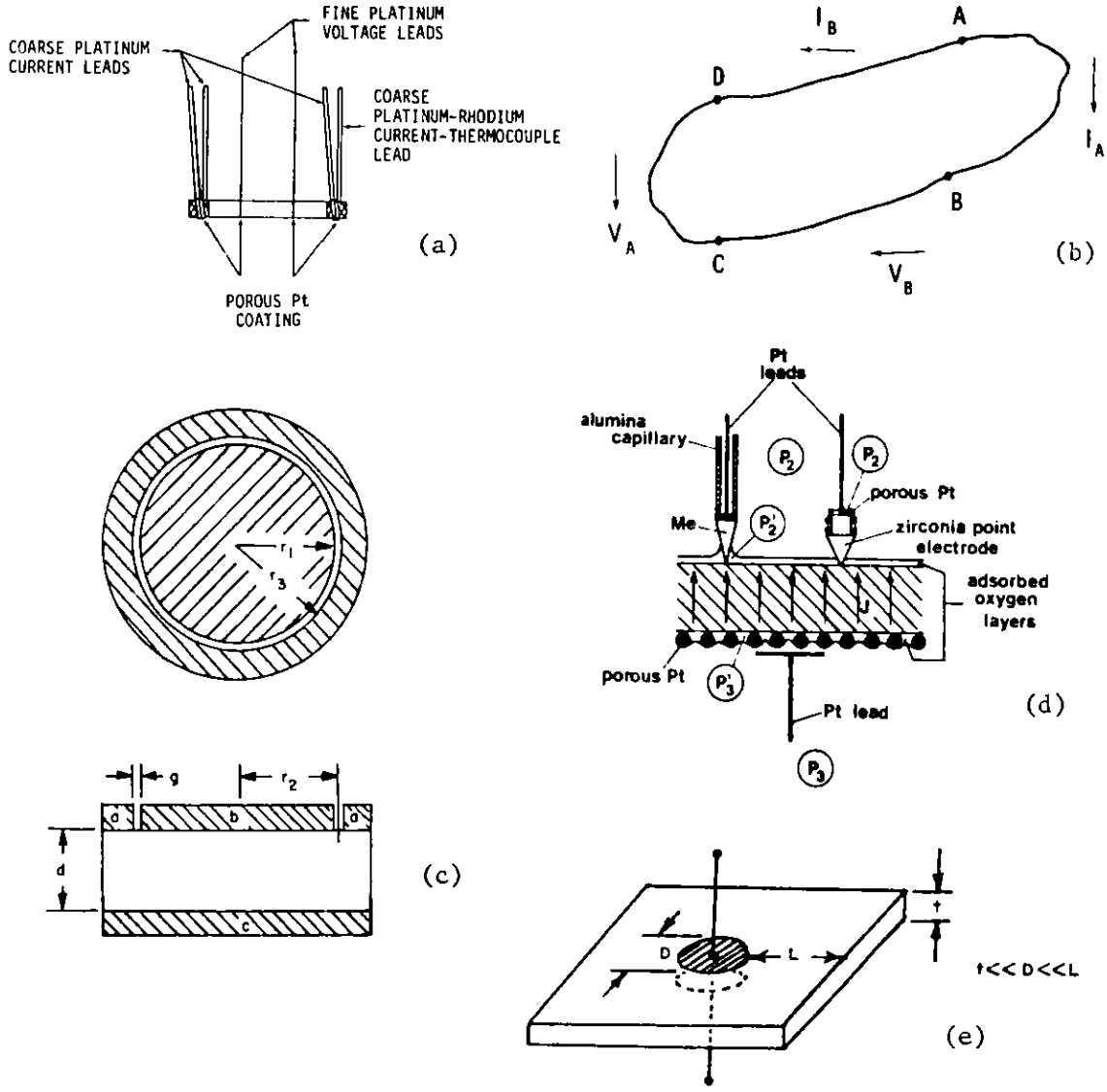

Fig. 31. Electrode Configurations. (a) Four-pole;[13] (b) four-pole van der Pauw;[16] (c) three-pole guarded;[16] (d) three-pole point electrode;[12] and (e) two-pole.[16]

electrode design. Reversible electrodes must have an ion in common with the conductor, if it is an ionic conductor, and any reactions involving electrons and ions at the interface must be free to occur.[18]

The dependencies of conductivity on chemical potential in oxides have been thoroughly discussed as crystalline defects.[19] The chemical potentials in the oxides are fixed by controlling the chemical potential of oxygen in the gas phase or with reversible electrodes. The exponential dependency of carrier concentration on 1/T is apparent from defect equilibria, with the possible exception of extrinsic nonassociated species and those oxides with significant band overlap such that conductivity is metallic in nature (e.g., some tungsten bronzes). In addition, mobilities show

thermal activation for ionic species and small polaron electronic species. Thus, precise temperature control is essential for reproducibility of the data. Additionally, at low signal levels, spatial nonuniformity of temperature distribution within the sample will lead to erroneous voltage in a volt-ampere measurement of conductivity.

b. Total Conductivity Measurement

The most effective electrode arrangement depends on the level of conductivity of the sample and the objectives of the measurement. Concomitant consideration must be given to the type of carrier and test signal available. A highly conducting specimen may require a four-probe technique to eliminate contact resistance, and, at high temperatures, lead resistances in the environmental chamber. In measurements on ionic conductors, dc electrode polarization can lead to artificially high sample resistances in two- or three-pole methods. This polarization can be relaxed by use of an ac measurement signal.[12] Consider Bauerle's model for the solid electrode-plus-electrode cell, as shown in Fig. 32a, where R is a resistor and C is a capacitor with frequency f. The complex admittance plot is shown in Fig. 32b, where G and B are the real and imaginary portions, respectively, of the admittance, y. Above the frequency represented by the peak of the first semicircle, the sluggishness of the electrode process (represented by the capacitance C_1 and resistance R_1) is relaxed. Therefore, G_2 represents the conductance of the sample and may represent the best dc performance which can be expected with very efficient electrodes.

In ceramics of low conductivity, surface conduction paths may be significant while electrode contributions to cell resistance may be negligible. Thus, a two- or three-probe technique might be more useful, especially if one or both electrodes are reversible, for subsequent electronic conductivity or ionic transference number measurements on the same sample. The third probe may be a guard ring or a volume guard. At very high temperatures, electrode-gas conductance may become significant,[17] and a volume guard is required. The guards are driven by a unity gain amplifier so that the potential is the same as the electrode which it surrounds. Thus, surface or electrode-gas current flows are drained without getting into the external measurement circuit which connects the surrounded electrode with the opposing electrode. For samples of intermediate conductivity, sometimes a very long surface path is sufficient protection from surface currents, such as indicated in Fig. 31e by the relative sample and electrode dimensions.

The control of chemical potential is accomplished either by gas-phase equilibration or by coexistence electrodes consisting of two phases of different composition but equal oxygen activity. In order to ensure equilibration with a gas phase, the gas phase must be well buffered (e.g., the equilibrating species content and flow rate must accommodate the mass flow required to reach equilibration). Also, in either case, precautions must be taken to ensure equilibrium is reached in the sample. The precautions include (1) adequate time at temperature and chemical potential to ensure equilibration, (2) slow cooling rates to avoid "quenched-in" defects during changing test temperature, and (3) approach to a set of conditions from higher and lower values.

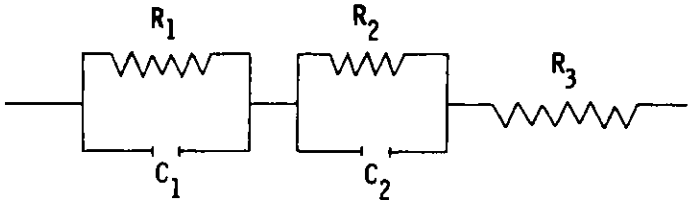

a. Equivalent Circuit

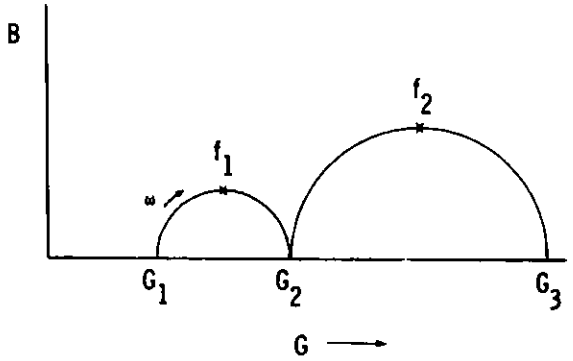

b. Complex Admittance Diagram

$$R_1 = \frac{1}{G_1} - \frac{1}{G_2} \qquad C_1 = \frac{G_2^2}{2\pi f_1 (G_2 - G_1)}$$

$$R_2 = \frac{1}{G_2} - \frac{1}{G_3} \qquad C_2 = \frac{G_3^2}{2\pi f_2 (G_3 - G_2)}$$

$$R_3 = \frac{1}{G_3}$$

Fig. 32. Equivalent Circuit Model of Solid Oxide Electrolyte Cell from Bauerle[12] and Corresponding Complex Admittance Plot, Y = G + jB

c. Determining the Contributions of Different Carrier Species

The techniques for separating the contributions of ionic species to conductivity from those of electronic species can be classified by the following electrode arrangement schemes: (1) both electrodes reversible to ionic species and electronic species, (2) one electrode reversible to ionic species and electronic species and one electrode reversible to electronic species and blocking to ionic species, and (3) both electrodes blocking to ionic species but reversible to electronic species. The electroding schemes cited above refer to the measuring electrodes. A third electrode reversible to electronic species may be included as a guard as indicated in the description of total conductivity measurements.

There are two approaches with two reversible electrodes: electrolysis and open-circuit EMF measurements. The electrolysis method as described by Tubandt,[20] Blumenthal and Seitz,[18] and Bottelberghs[21] consists of placing the sample between two identical reversible electrodes containing one component of the sample. The current transfer is measured with a coulometer. The mass transport between the electrodes is then measured by gravimetric analysis, digestion, and quantitative chemical analysis, or electron microprobe analysis of the sectioned electrodes.[21] The open-circuit EMF measurements are based on the irreversible thermodynamic analysis given by Wagner[22] for a cell:

$$\text{metal}/O_{2(\mu'_{O_2})} \;|\text{oxide sample}|\; O_{2(\mu''_{O_2})}/\text{metal}$$

The measured EMF is given by

$$E = \frac{1}{4F} \int_{\mu'_{O_2}}^{\mu''_{O_2}} t_{ion} d\mu_{O_2}, \qquad (2)$$

where t_{ion} is the ionic transference number, the sum of the partial conductivities due to the ionic species divided by the total electrical conductivity of the sample. Schmalzreid[23] shows solutions for various forms of the dependency of ionic transference number on oxygen partial pressure. The ionic transfer number is frequently approximated as a constant for closely spaced values of μ'_{O_2} and μ''_{O_2}.[20] Several schemes have been used to fix the oxygen potential of the electrodes including mixtures of gases such as CO/CO_2 or solid state electrodes consisting of two phases of differing oxidation states of a metal. There are two types of methods involving electrodes blocking to ionic species which yield the conductivity of an oxide due to electrons and holes. Vest and Tallan[17] used a sample arrangement with two blocking electrodes and observed the decay of dc conductivity with time. The steady-state conductivity was attributed to the electronic (electron and hole) species. This was then compared to the total conductivity as measured by either extrapolating to zero time or by dc measurements. The problem with using two blocking electrodes appears when conductivity is a function of oxygen chemical potential, in that establishing a reference oxygen potential to

correlate to the measured conductivity is difficult. Another approach is the use of one electrode which is reversible to ionic species and fixes oxygen chemical potential and one electrode which is blocking to ionic species. The partial conductivities due to electrons and holes are derived from analysis of the voltage dependency of the steady-state conductivity of the oxide sample. The equations for this analysis were developed by Wagner[24] on the basis of zero ionic current. Patterson, Bogren, and Rapp[25] developed specific forms of these equations for calcia-stabilized zirconia and yttria-doped thoria and applied the method experimentally. Their expression for total current density with the ionic current blocked is

$$J = \frac{kT}{qL}\ \sigma_e^o \left\{ [1 - \exp(-q\,E/kT) + \sigma_h^o\ [\exp(qE/kT) - 1] \right\}$$

where J = current flux,

k = Boltzmann constant,

T = temperature (K),

q = charge of the electron,

L = length of conduction,

E = applied voltage, and

σ_e^o, σ_h^o = partial conductivities of electrons and holes at the chemical potential of the reversible electrode.

Dividing through by [1 - exp (-qE/kT)] transforms this equation into a slope/intercept form so that the partial conductivities can thus be determined by a linear fit.

Thermoelectric effect is readily usable in electronic conductors for determining the sign of the carrier species. The chemical potential of carriers with equal numbers of donors (or acceptors) at the hot and cold ends is higher at the hot end. Therefore, the carrier species migrates to the cold end, resulting in an electrical potential gradient with the sign of the cold end being the same as the sign of the carrier species charge. For ionic carrier species, the analysis of experimental data is more difficult[26] because the enthalpies of the half-cell reactions at the electrodes must be taken into consideration in the heterogeneous portion of the Seebeck coefficient of the cell.

d. Microstructural Effects and Electrode Behavior

The behavior of polycrystalline ionic conductors and their electrodes can be characterized by ac measurements according to the methods of Bauerle.[12] He found that the equivalent circuit of Fig. 32a applied generally well to the cell:

$$Pt/O_2\,|\,(CaO)ZrO_2\,|\,Pt/O_2$$

The ac dispersion of conductance gives semicircular plots of complex admittance as shown in Fig. 32b. These plots can be analyzed to give the effective values of resistance and capacitance in the equivalent circuit. The rate of the electrode reaction seems to be reflected in R_1, but the physical meaning of C_1 is not clear. Both R_2 and C_2 are properties of grain boundaries or distributed minority second phase. The resistance of the bulk grain material is R_3. Practically speaking, the sum of resistances R_2 and R_3 is the material property to be considered for a solid electrolyte under dc operation as in a fuel cell. However, separation of these parameters can help in optimizing microstructural and processing variables in the electrolyte for best performance.

Another approach to measuring electrode performance has been used in oxygen gauges by Fouletier, Fabry, and Kleitz.[14] The overvoltage at the electrode/electrolyte interface was measured by using a third reference electrode made of a "point" of solid electrolyte material in contact with the solid electrolyte membrane, as shown in Fig. 31d. This probe can be used to examine the difference between the voltage at the working electrode/electrolyte interface and theoretical voltage at the oxygen potential of the bulk electrode gas. This technique was used to examine electrode overpotentials due to leakage currents through the membrane. However, the concept could also be applied to examining electrode performance while current is drawn through a reference electrode and the electrode type being studied.

REFERENCES

1. R. D. Pierce et al., Advanced Fuel Cell Development Quarterly Progress Report, January-March 1982, Argonne National Laboratory Report ANL-83-34, pp. 11, 12, 29-34 (August 1983).

2. R. D. Pierce et al., Advanced Fuel Cell Development Quarterly Progress Report, October-December 1981, Argonne National Laboratory Report ANL-82-68 (April 1983).

3. T. D. Kaun, Solubility of the NiO Fuel Cell Cathode in Li_2CO_3-K_2CO_3 Melts as Determined by Cyclic Voltammetry, Fourth Int. Symp. on Molten Salts, The Electrochemical Society (1983).

4. R. D. Pierce et al., Advanced Fuel Cell Development Quarterly Progress Report, April-June 1980, Argonne National Laboratory Report ANL-80-98 (November 1980).

5. R. D. Pierce et al., Advanced Fuel Cell Development Quarterly Progress Report, January-March 1981, Argonne National Laboratory Report ANL-81-68 (October 1981).

6. C. E. Scott and J. S. Reed, Effect of Laundering and Milling on the Sintering Behavior of Stabilized ZrO_2 Powders, Bull. Amer. Ceram. Soc. 58, 587-590 (1979).

7. P. H. Rieth and J. S. Reed, Fabrication and Flexural Strength of Ultrafine-Grained Yttria-Stabilized Zirconia, ibid. 55, 717-727 (1976).

8. R. B. Poeppel, Argonne National Laboratory, private communication (1983).

9. C. E. Scott and J. S. Reed, Analysis of Cl^- Ions Laundered from Submicron Zirconia Powders, Bull. Amer. Ceram. Soc. 57, 741-743 (1978).

10. M. Pechim, Method of Preparing Lead and Alkaline Earth Titanates and Niobates and Coatings Using the Same to Form a Capacitor, U.S. Patent 3,300,697, (July 1967).

11. Advanced Fuel Cell Development Progress Report for January-March 1983, Argonne National Laboratory Report, in preparation.

12. J. E. Bauerle, J. Phys. Chem. Solids 30, 2657-2670 (1969).

13. G. E. Pike and G. H. Seager, J. Appl. Phys. 50(5), 3414-3422 (1979).

14. J. Fouletier, P. Fabry, and M. Kleitz, J. Electrochem. Soc. 123(2), 204-213 (1976).

15. R. A. Rapp and D. A. Shores, Techniques of Metals Research, Vol. IV, Part 2, R. A. Rapp, Ed., pp. 123-192 (1970).

16. L. J. van der Pauw, Philips Res. Rep. 13(1), 1-9 (1958).

17. R. W. Vest and N. M. Tallan, J. Appl. Phys. 36, 543 (1965).

18. R. N. Blumenthal and M. A. Seitz, in Electrical Conductivity in Ceramics and Glass, Part A, N. M. Tallan, ed., M. Dekker, NY, pp. 35-178 (1974).

19. R. J. Brooke, ibid., pp. 179-267.

20. C. Tubandt, Handbook der Experimental-Physik, X. Weis and X. Harm, Eds., Vol. 12, Part II, Academische Verlagsgesellschaft.

21. P. H. Bottelberghs, Solid Electrolytes: General Principles, Characterization, Materials, Applications, P. Hagenmuller and W. Van Gool, Eds., Academic Press, NY, pp. 145-172 (1978).

22. C. Wagner, Zeitschrift fur Physikalische Chemie Abt. B, Vol. 21, p. 25 (1933).

23. H. Schmalzreid, Z. fuer Phys. Chem., N.F., Vol. 38, pp. 87-102 (1936).

24. C. Wagner, International Committee of Electrochemical Thermodynamics and Kinetics, Seventh Meeting, Butterworths, London, pp. 361-371 (1957).

25. J. W. Patterson, E. L. Bogren, and R. A. Rapp, J. Electrochem. Soc. 114(7), 752-758 (1967).

26. R. J. Ruka, J. E. Bauerle, and L. Dykstra, J. Electrochem. Soc. 115, 497-501 (1968).

Distribution for ANL-83-89

Internal:

J. P. Ackerman
P. A. Blackburn
R. L. Breyne
L. Burris
T. D. Claar
G. M. Cook
D. W. Dees
J. T. Dusek
D. C. Fee
P. A. Finn
B. K. Flandermeyer
A. V. Fraioli
J. E. Harmon
A. A. Jonke
T. D. Kaun
M. Krumpelt
G. H. Kucera
N. Q. Minh
F. C. Mrazek
Z. Nagy
P. A. Nelson
J. J. Picciolo
R. D. Pierce (15)
R. B. Poeppel
J. J. Roberts
J. L. Smith
J. R. Stapay
R. K. Steunenberg
E. H. VanDeventer
J. E. Young
S. A. Zwick
A. B. Krisciunas
ANL Patent Dept.
ANL Contract File
ANL Libraries (3)
TIS Files (6)

External:

DOE-TIC, for distribution per UC-93 (139)
Manager, Chicago Operations Office, DOE
R. J. Gariboldi, DOE-CH
Chemical Engineering Division Review Committee Members:
- T. Cole, Jet Propulsion Lab.
- W. L. Worrell, U. Pennsylvania

Materials Science Division Review Committee:
- C. B. Alcock, U. Toronto
- A. Arrott, Simon Fraser U.
- R. C. Dynes, Bell Labs., Murray Hill
- A. G. Evans, U. California, Berkeley
- L. M. Falicov, U. California, Berkeley
- H. K. Forsen, Bechtel Group, Inc., San Francisco
- E. Kay, IBM San Jose Research Lab.
- M. B. Maple, U. California-San Diego
- C. L. McCabe, Cabot Corp., Kokomo, Ind.
- P. G. Shewmon, Ohio State U.
- J. K. Tien, Columbia U.

B. S. Baker, Energy Research Corp., Danbury, Conn.
R. W. Barta, General Electric Co., Ballston Spa, N. Y.
J. L. Bates, Pacific Northwest Lab.
T. R. Beck, Electrochemical Technology Corp., Seattle
R. Bradley, Oak Ridge National Lab.
E. Camara, Inst. Gas Technology, Chicago
P. T. Carlson, Oak Ridge National Lab.
T. W. Carter, U. S. Coast Guard, Washington
D. Chatterji, General Electric Co., Schenectady
J. Cuttica, Gas Research Inst., Chicago
W. Feduska, Westinghouse R&D Center, Pittsburgh
L. M. Ferris, Oak Ridge National Lab.
A. P. Fickett, Electric Power Research Inst.
E. Gillis, Electric Power Research Inst.
J. Giner, Giner, Inc., Waltham, Mass.
F. Gmeindl, Morgantown Energy Technology Center
G. L. Hagey, Div. Advanced Energy Conversion Systems, USDOE
J. W. Harrison, General Electric Co., Wilmington, Mass.

L. C. Headley, Morgantown Energy Technology Center
D. T. Hooie, Gas Research Inst., Chicago
A. O. Isenberg, Westinghouse R&D Center, Pittsburgh
D. Johnson, Northwestern U.
J. Kelly, Westinghouse R&D Center, Pittsburgh
C. Kinney, Office of Fossil Energy, USDOE
K. Kinoshita, Lawrence Berkeley Lab.
H. R. Kunz, United Technologies Corp., South Windsor, Conn.
A. R. Maret, Gas Research Inst., Chicago
N. Margalit, Combustion Engineering, Windsor
L. Marianowski, Inst. of Gas Technology, Chicago
H. Maru, Energy Research Corp., Danbury, Conn.
R. Matsumato, Ceramatech, Salt Lake City
A. P. Meyer, United Technologies Corp., South Windsor, Conn.
C. A. Reiser, United Technologies Corp., South Windsor, Conn.
F. Salzano, Brookhaven National Lab.
J. Searls, U. S. Bureau of Mines, Washington
R. Selman, Illinois Inst. of Technology
J. Sholes, Morgantown Energy Technology Center
J. W. Sim, Kinetic Systems Corp., Lockport, Ill.
P. Stonehart, Stonehart Associates, Inc., Madison, Conn.
G. Wilemski, Physical Sciences Inc., Andover, Mass.
K. Wray, Physical Sciences Inc., Andover, Mass.
E. Yeager, Case Western Reserve U.
C. Zeh, Morgantown Energy Technology Center, USDOE